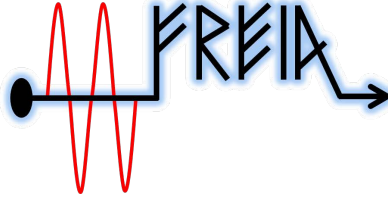


Accelerator Development at the FREIA Laboratory

R. Ruber, A.K. Bhattacharyya*, D. Dancila, T. Ekelöf, J. Eriksson, K. Fransson,
K. Gajewski, V. Goryashko, L. Hermansson, M. Jacewicz, M. Jobs, Å. Jönsson,
H. Li, T. Lofnes, A. Miyazaki, M. Olvegård, E. Pehlivan,
T. Peterson, K. Pepitone, A. Rydberg, R. Santiago Kern, R. Wedberg,
A. Wiren, R. Yogi*, V. Ziemann

FREIA Laboratory,
Department of Physics and Astronomy,
Uppsala University, Uppsala, Sweden

March 10, 2021



Abstract

The FREIA Laboratory at Uppsala University focuses on superconducting technology and accelerator development. It actively supports the development of the European Spallation Source, CERN, and MAX IV, among others. FREIA has developed test facilities for superconducting accelerator technology such as a double-cavity horizontal test cryostat, a vertical cryostat with a novel magnetic field compensation scheme, and a test stand for short cryomodules. Accelerating cavities have been tested in the horizontal cryostat, crab-cavities in the vertical cryostat, and cryomodules for ESS on the cryomodule test stand. High power radio-frequency amplifier prototypes based on vacuum tube technology were developed for driving spoke cavities. Solid-state amplifiers and power combiners are under development for future projects. We present the status of the FREIA Laboratory complemented with results of recent projects and future prospects.

*Present affiliation European Spallation Source, Lund, Sweden

1 Introduction

In May 2009 the European research ministers agreed to build the next large European research infrastructure, the European Spallation Source (ESS), in Sweden. Since, at that time, the ESS had limited personnel, Swedish universities were called upon to participate. Uppsala University was particularly suitable to respond to this call, because it had operated the Gustav-Werner cyclotron since the late 1940s [1] and later the CELSIUS cooler ring [2] with the WASA detector [3]. In recent times Uppsala University had participated in CTF3 at CERN [4] and in FLASH [5] and XFEL [6], both at DESY. Moreover, experience with cryogenics and superconducting magnets [7, 8] was available, which was particularly useful considering that ESS uses superconducting acceleration structures.

The scope of the collaboration between ESS and Uppsala University was agreed to comprise the design of a radio-frequency (RF) power generation and distribution system, as well as testing all components, including superconducting RF accelerator cavities. This stimulated the construction of a complete test-stand in Uppsala, similar to CHECHIA [9], CRYHOLAB [10], or HoBiCat [11]. The focus of the new facility became spoke type superconducting RF cavities for which no other high-power test stand is available in Europe. These types of superconducting cavities, also known as spoke resonator, were first proposed in the late 1990s [12] but the ESS will be the first large infrastructure to use them. For ESS, these cavities have two spokes, resulting in three acceleration gaps, and are referred to as double-spoke cavities. They accelerate the proton beam from 90 MeV kinetic energy at the output of the normal conducting section of the accelerator to 220 MeV at the input of the elliptical cavity section of the accelerator.

The new facility was formally established in 2011 and named FREIA (Facility for Research Instrumentation and Accelerators). The layout of the laboratory is shown in figure 1 with bunkers for the horizontal cryostat in the center of a newly erected 1000 m² building. The site of the laboratory

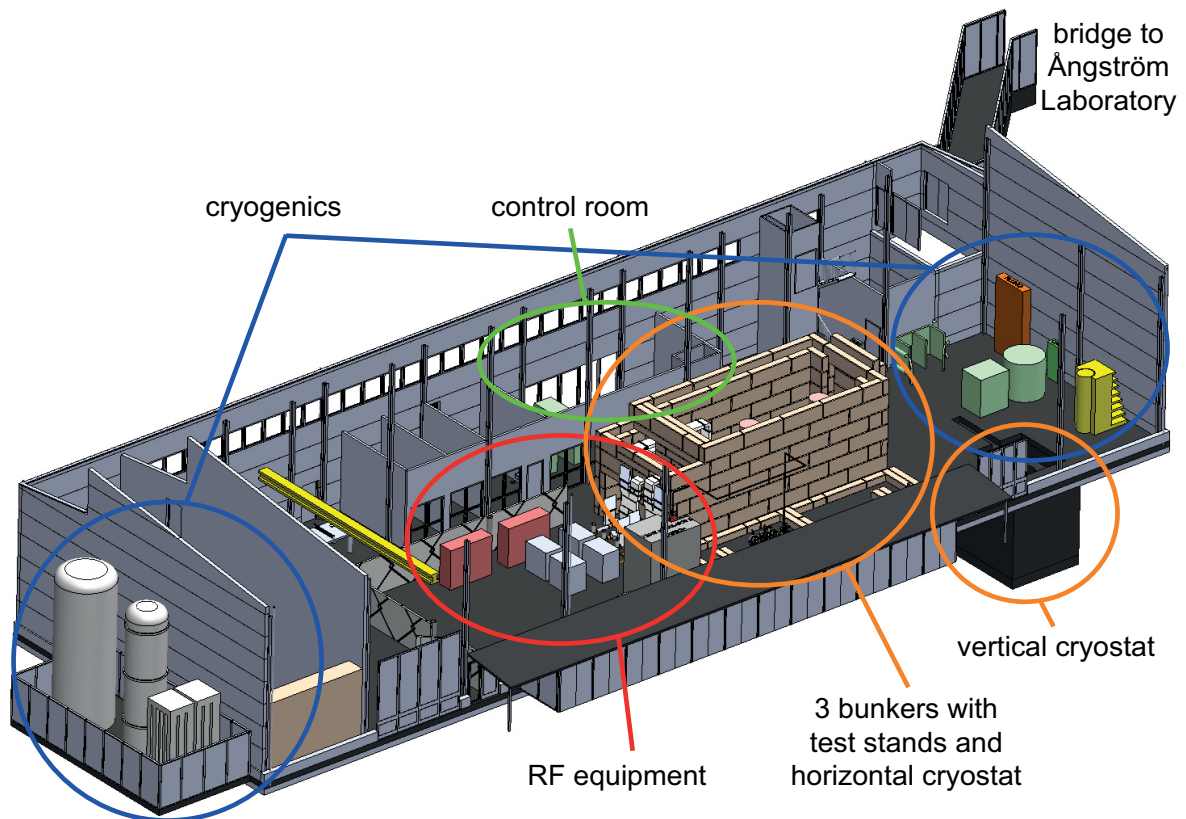


Figure 1: Layout of the FREIA Laboratory.

was decided to be placed adjacent to the Ångström Laboratory, the present site of the physics, engineering and chemistry departments. Construction of the new laboratory building was completed in 2013.

The basic layout of the test areas includes the superconducting accelerating cavities, high-power RF source, RF distribution, and controls system. The central part of the laboratory comprises a horizontal cryostat that can accommodate one or two superconducting cavities. The cryostat has to be located in a concrete bunker for radiation protection purposes and is cooled by a cryogenic system providing liquid helium and liquid nitrogen; all is supervised by an integrated controls and monitoring system. Additional space is allocated inside the bunker for the testing of cryomodules, which are specialized cryostat-modules, with one or multiple accelerating cavities, that are installed in the final accelerator itself. The RF power stations are placed outside of the bunker, adjacent to its western side. Due to an architectural intervention, the cryogenic system ended up on the eastern end of the building while the helium compressor and gas storage ended up on the western end. Control room, workshops, and storage areas are on the ground level with office space above.

An optional vertical cryostat was considered from the beginning as the simplest way for future testing of superconducting cavities. This idea was later updated for multi-purpose superconducting cavity and magnet testing, and the cryostat was finally added in 2019.

In the following sections we walk the reader through all parts, starting with the cryostats, which occupy a central role for testing components, and the associated cryogenics system. This is followed by a section on the power generation and distribution, which served as a prototype for part of the ESS system. Then we address the test infrastructure and present recent results. Finally, we discuss upcoming and future activities.

2 Cryostats

The horizontal cryostat “Hnoss¹” is dedicated to test superconducting cavities and located inside a radiation protection bunker next to a test stand for testing cryomodules for the ESS. Our vertical cryostat “Gersemi¹,” is located in a vertical shaft and used to test both superconducting cavities and magnets.

2.1 “Hnoss”, The Horizontal Cryostat

The outer housing of Hnoss is a stainless steel cylinder with large doors at its ends and a valve box on top, as shown in figure 2. Multiple vacuum flanges are available to mount feedthroughs for signal cables and to connect power couplers for the RF, either from the left, right, top or bottom. With its inner length of 3.3 m and diameter of 1.2 m, Hnoss is large enough to accept two superconducting cavities with their individual liquid helium reservoirs and with power couplers installed. In particular, Hnoss can accommodate two ESS-type 352 MHz double-spoke cavities, but also two 704 MHz ESS-type elliptical cavities or two TESLA/ILC-type 1.3 GHz cavities [13].

Inside the vessel a mu-metal sheet reduces the Earth-magnetic field by a factor of 5 and an aluminium sheet functions as thermal-radiation shield while cooled with liquid nitrogen to about 80 K [14]. The superconducting cavities, or any other devices under test, are cooled by liquid helium to temperatures between 1.8 and 4.2 K. The cavities are either suspended from the outer vessel wall by tie-rods or supported by a liquid helium cooled table that is placed at the bottom of the cryostat. This table is equipped with rails to simplify installation work, but it can also be removed to create more space for larger cavities.

An interconnection box inside the bunker routes the liquid helium, arriving from the liquefier at about 1.2 bar, to the valve box on top of the Hnoss cryostat. This cooling circuit is shown in figure 3. The yellow boxes represent different sub-systems. Liquid helium and nitrogen arrive through the interconnection box into the valve box which sits on top of the horizontal cryostat itself. Inside the

¹In Nordic mythology, Hnoss and Gersemi are daughters of the goddess Freia.

valve box the helium enters a small storage dewar, called the 4K pot, from where it can be routed directly to the cavities (or any other device under test), during initial cool down at 4 K, and to the support table. A third route passes the 4 K Helium via a heat exchanger to a Joule-Thomson valve, where the helium temperature is lowered by isenthalpic expansion. The resulting helium, at temperatures down to 1.8 K, is collected in a second dewar, called the 2K pot, from where it is delivered to the cavities [15]. A bypass line for the Joule-Thomson valve allows us to operate fully in 4 K mode. After having cooled the cavities, the returning gas passes the cold side of the previously mentioned heat-exchanger to pre-cool helium on its way to the Joule-Thomson valve. The return gas leaves the valve box through a port on the top from where it passes a heater system, located outside the bunker, which increases the gas temperature to ambient temperature before entering sub-atmospheric pumps that lower the pressure to values required for the desired outlet temperature at the Joule-Thomson valve.

The valve box also contains circuits for liquid nitrogen to cool the thermal shield of the cryostat. The RF couplers of the cavities can be cooled either by the liquid nitrogen or by 5 K supercritical helium. The supercritical helium is produced in a secondary helium circuit that is cooled by an additional heat exchanger on the exhaust of the 2K pot. The helium gas in this secondary circuit is fully separated from the helium gas circuit of the cryogenic plant.

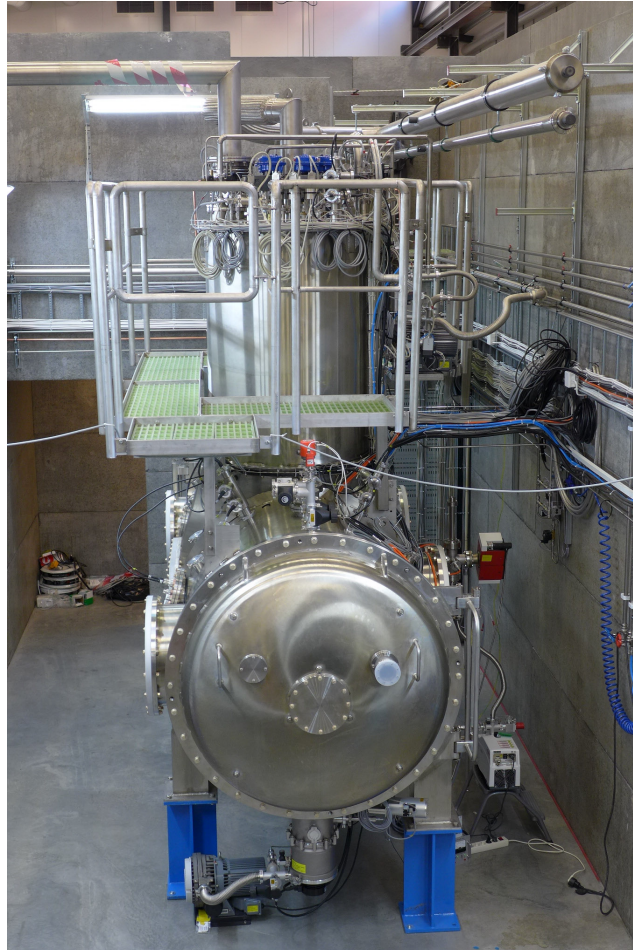


Figure 2: The Hnoss horizontal cryostat, looking towards one of its loading doors, with the cryogenic valve box, surrounded by a maintenance platform, on its top. Insulation vacuum pumps can be seen below.

2.2 Cryomodule Test Stand

Inside the bunker, adjacent to Hnoss, space is available to test ESS cryomodules. The same interconnection box that also supplies Hnoss, delivers liquid helium and liquid nitrogen to a valve box that is located next to the cryomodule; a setup that mimics the installation in the ESS accelerator. Figure 4 shows a prototype valve box and cryomodule for spoke cavities installed in the bunker. A similar cryogenic flow principle is used as for Hnoss: the 2 K helium from the valve box is routed to the cryomodule, where it cools two spoke-cavities. After leaving the cryomodule, the return gas passes through the same heater and the same sub-atmospheric pumps that are used for Hnoss in order to lower the pressure to values needed to operate the Joule-Thomson valve in the valve box.

Valve box and cryomodule are rolled into position using a trolley by entering the bunker through a demountable wall at the backside of the bunker, opposite to the side facing the RF stations. For the series acceptance testing of ESS cryomodules the same valve box will remain in place for all tests.

2.3 “Gersemi”, The Vertical Cryostat

The construction of Gersemi resembles that of Hnoss and is connected to the same sub-atmospheric pumps. Only, in Gersemi, the valve box with the Joule-Thomson valve to provide 2 K helium shown on the top-left in figure 5 is standing next to a 5 m deep shaft that has a diameter of 2 m. This shaft contains the stainless steel vessel of the vertical cryostat itself, in which to test either superconducting

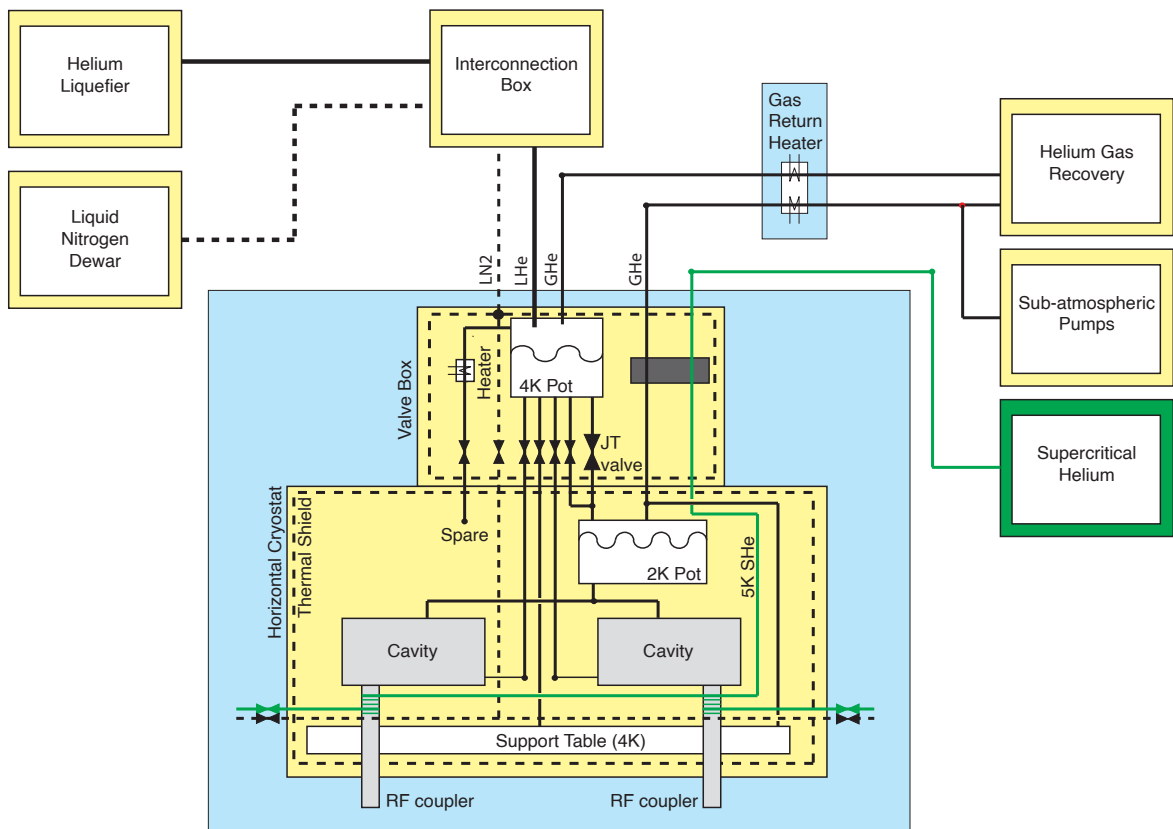


Figure 3: The cryogenic scheme of Hnoss with the valve box including the 4K pot on top of the horizontal cryostat with the cavities. Liquid nitrogen (LN2, dashed) is used to cool the thermal shield and RF couplers and liquid helium (LHe, solid) to cool the cavities and the support table. Gas helium return lines are marked “GHe”. The supercritical helium line (green) as alternative cooling for the RF couplers is marked “5K SHE”.

cavities or magnets. The top flange of the cryostat is visible near the bottom of figure 5. The space inside the cryostat is limited to a height of 3.05 m and a diameter of 1.1 m. Moreover, in order to test magnets in a pressurized 2K helium bath, a so-called lambda-plate separate the 2K helium bath from a 4K bath above. The available height below the lambda-plate is 2.65 m.

Gersemi supports three operational modes: (1) saturated liquid bath, (2) sub-cooled bath for magnets, and (3) vacuum. So-called “inserts” are used for testing a device with each operational mode having its own insert type shown in figure 6. An insert is in fact the top flange of the cryostat with a mechanical support for suspending the device to be tested. The insert includes feedthroughs for all necessary connections: cryogenics, vacuum, signals etc.

In mode 1, bare cavities without surrounding helium container are directly placed in a saturated liquid bath with temperatures in the range of 1.8 to 4.5 K, depending on the pressure. The liquid helium supply is organized such that the cryostat is cooled down and filled from the bottom, and then shifts to the top during steady state operation. The cold helium gas returns through a heat exchanger in the valve box and connects either to the 2 K sub-atmospheric pumping system or via a bypass to the gas recovery system.

Mode 2 is used for superconducting magnets. The magnet is suspended below the lambda-plate in a pressurized 2K helium bath, while above the lambda-plate there is a saturated 4K helium bath. As in mode 1, the liquid helium supply is organized such that the cryostat is cooled down

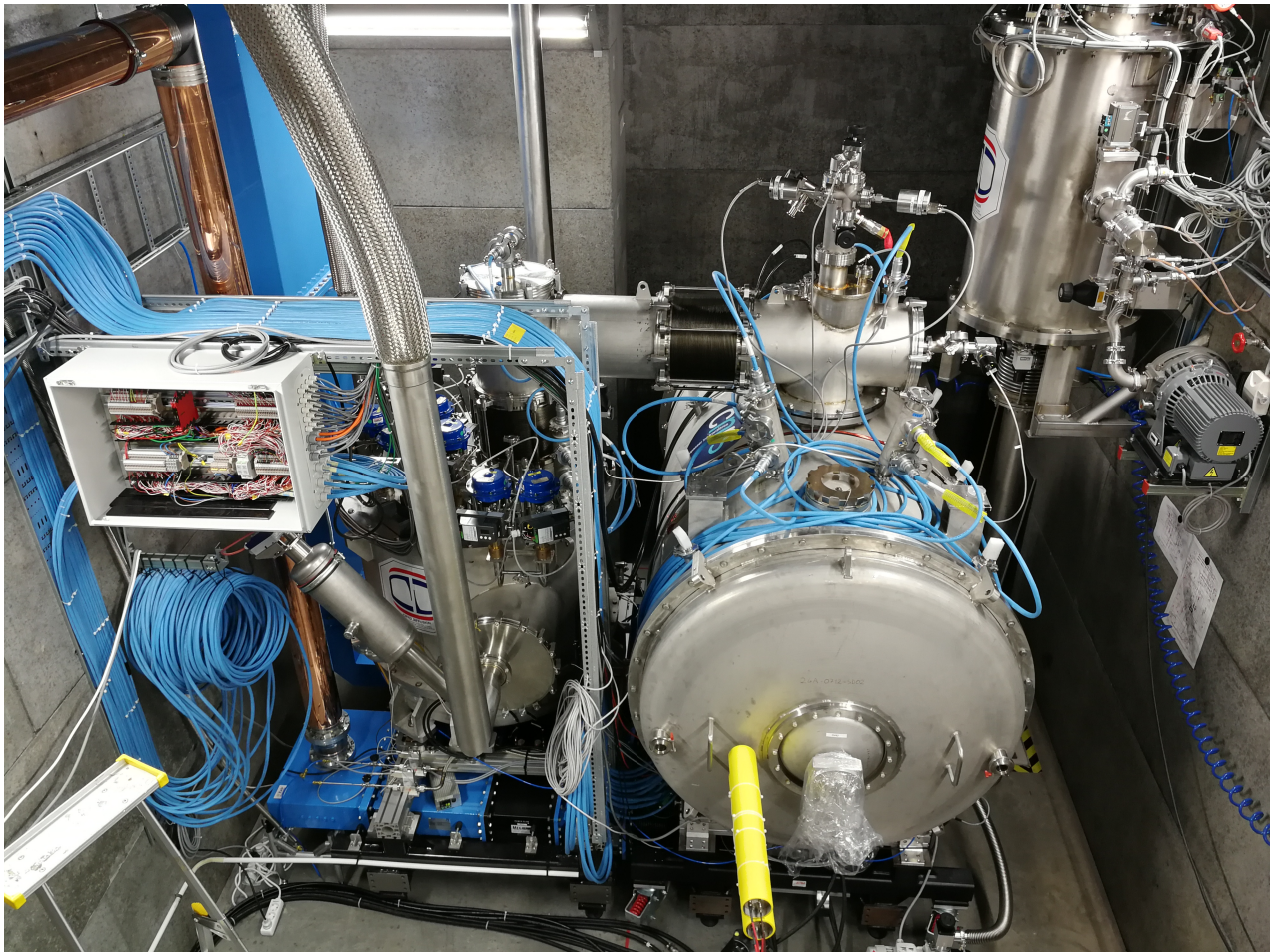


Figure 4: The test stand with an ESS cryomodule shown at the right and the valve box at the left. Liquid helium and liquid nitrogen arrive through the cryogenic interconnection box visible at the top-right. RF power arrives through the coaxial waveguide (copper coloured) and rectangular waveguide (blue) shown at the far-left.

and filled through the bottom, and then shifts to the top during steady state operation. To cool the bath below the lambda-plate, a fraction of the 4 K helium above the lambda-plate is pumped by the sub-atmospheric pumps through a heat exchanger and a Joule-Thomson valve. The helium continues through a second heat exchanger cooling the helium bath below the lambda-plate before flowing back through the first heat exchanger cooling the incoming 4 K helium [16]. A separate cold gas return line, passing through the valve box, is used for the 4 K bath itself.

Mode 3 is similar to the operation in Hnoss, where superconducting cavities, or any other devices, are equipped with a liquid helium vessel. In this mode of operation, the surrounding test volume of the cryostat is evacuated, hence the naming vacuum mode. The liquid helium supply is organized through valves in the cryostat that redirect the liquid helium through a short transfer line to the top of the insert and from there to the helium reservoir of the device being tested. The cold helium gas return connects through a heat exchanger in the valve box either to the 2 K sub-atmospheric pumping system or to a bypass to the gas recovery system. An additional transfer line can be used to supply liquid nitrogen if a separate thermal screen is installed for the insert. As this mode of operation is equivalent to testing in Hnoss, the hardware of the insert and transfer lines has not yet

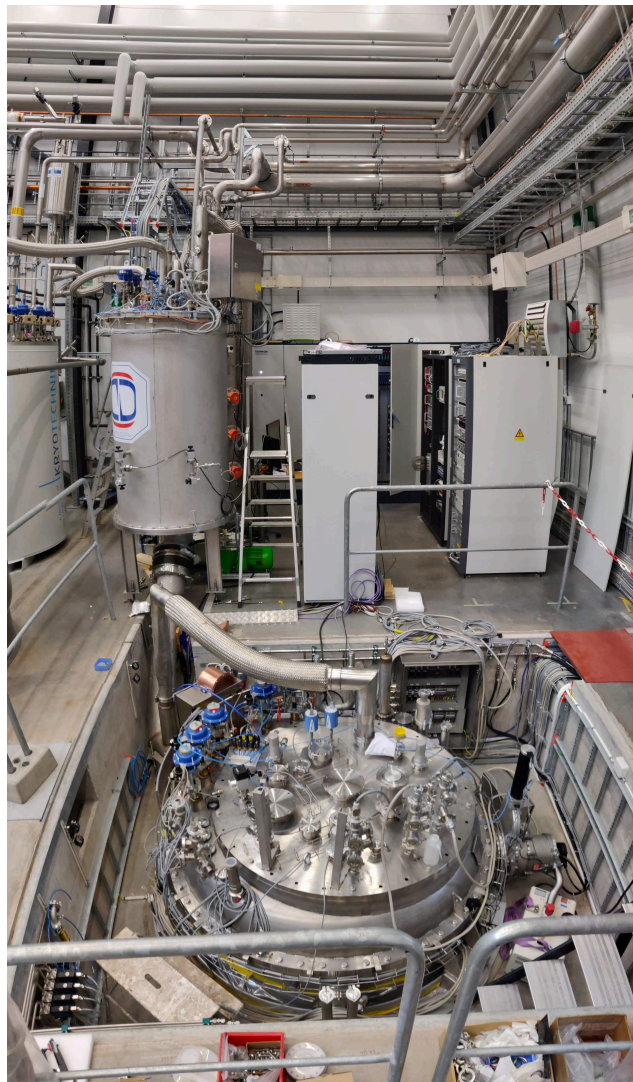


Figure 5: The Gersemi vertical cryostat inside its shaft with the valve box at the rear left. A transfer line for liquid helium and nitrogen connects from the bottom of the valve box to the left side of the cryostat and is partly hidden by the flexible transfer line for the return gas. The racks with power supplies and controls equipment are at the rear right.

been constructed.

Initially, a removable magnetic shield was foreseen outside the vacuum vessel. It was planned to use the shield when testing superconducting cavities and to remove it when testing superconducting magnets. Since such a magnetic shield would be rather fragile, we replaced it by an active earth-field compensation magnetic system consisting of three horizontal and three vertical coils that surround the vessel of the cryostat [17]. Three horizontal coils, spaced 1 m apart, produce a reasonably constant vertical field component, provided they are excited in a 1, 2/3, 1 pattern. We found this configuration by optimizing the field flatness over 1.6 m and picked an integer wiring ratio with small numbers of 8 and 12 windings for the center and end-coils, respectively. The three vertically mounted coils have a height of 3.7 m and can be powered independently to provide any horizontal field component. The field quality within a circle of 0.4 m radius is below $4 \mu\text{T}$ at an excitation of $60 \mu\text{T}$, or below 3% [18].

3 Cryogenic System

A schematic overview of the liquid nitrogen and liquid helium cryogenic system is shown in figure 7. A helium liquefier supplies an intermediate storage dewar from which the liquid helium is distributed to Gersemi and to an interconnection box which in turn supplies Hnoss and the cryomodule test stand [19]. The helium gas returns directly to the recycle compressor of the helium liquefier, or to the sub-atmospheric pumping and gas recovery systems. In parallel, liquid nitrogen is used for pre-cooling

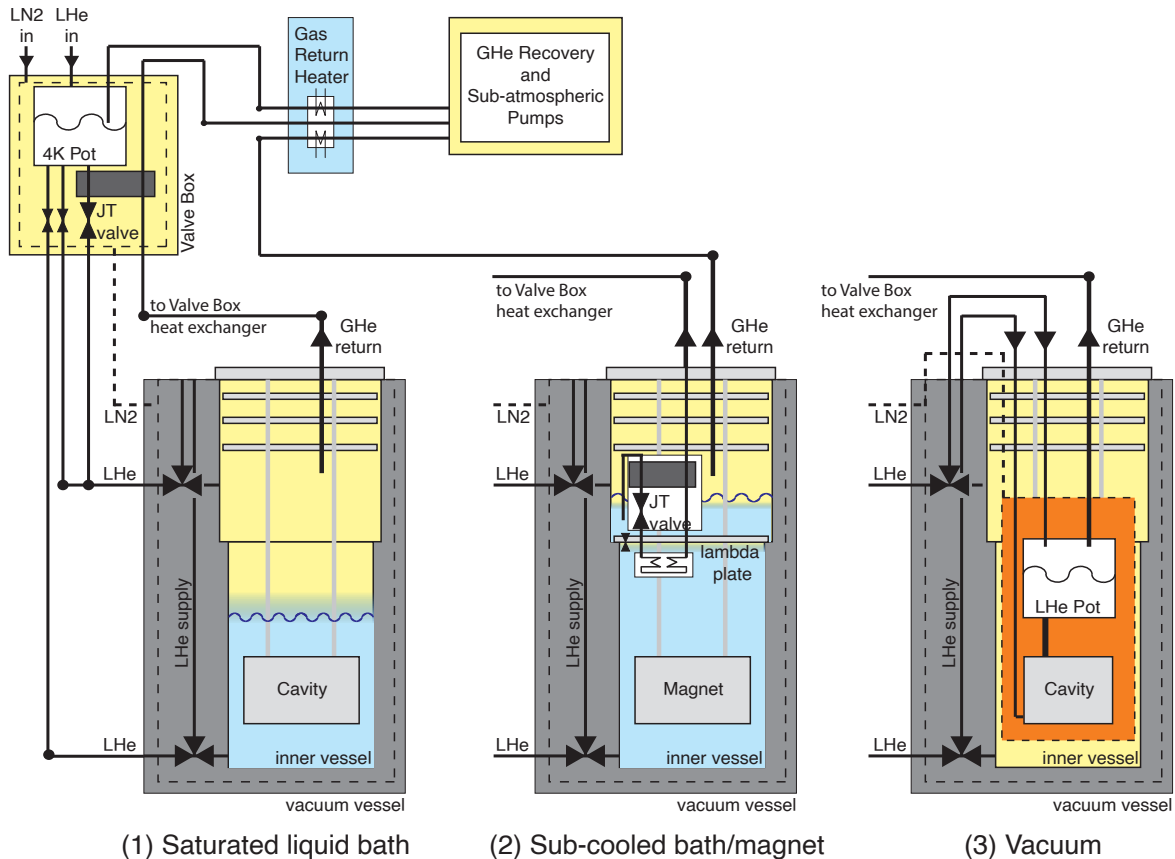


Figure 6: Gersemi’s three operational modes and insert types: liquid, magnet, and vacuum. Liquid helium and nitrogen from the valve box (top left) enter the cryostat (gray) from the left, where valves are used to orchestrate the helium flow for the three operation modes. The magnet mode uses two gas helium return lines: one for the helium bath above and one for below the lambda plate.

of the liquefier cold box and cryostat thermal shields. The main parameters of the cryogenic system are listed in table 1.

Over 50,000l liquid nitrogen and 8,000l liquid helium are distributed annually to external users at the university, other government agencies and private companies nearby. The liquid nitrogen is stored in a 20,000l medium pressure dewar at some 60m distance from the helium liquefier, therefore a phase-separator is used to reduce the pressure and remove any gas nitrogen at the end of the transfer-line.

3.1 Helium Liquefaction

The helium liquefier system consists of a recycle compressor and a cold box. The recycle compressor is a Kaeser screw compressor with a maximum discharge pressure of 14 bar. The cold box is a Linde L140 type containing the heat exchangers and expanders that cool down and liquefy the helium gas. A fraction of the gas flow from the recycle compressor is led through two turbines where the gas is cooled by adiabatic expansion. This gas flow is then used to cool down the heat exchangers which in turn cool down the remaining fraction of the gas flow. This high pressure cold gas then passes through a Joule-Thompson valve in an isenthalpic expansion process and is liquefied and stored in a 2000l dewar. A liquefaction rate exceeding 150l/h was reached with liquid nitrogen pre-cooling of the first heat exchanger in the cold box, and about half that rate without liquid nitrogen pre-cooling.

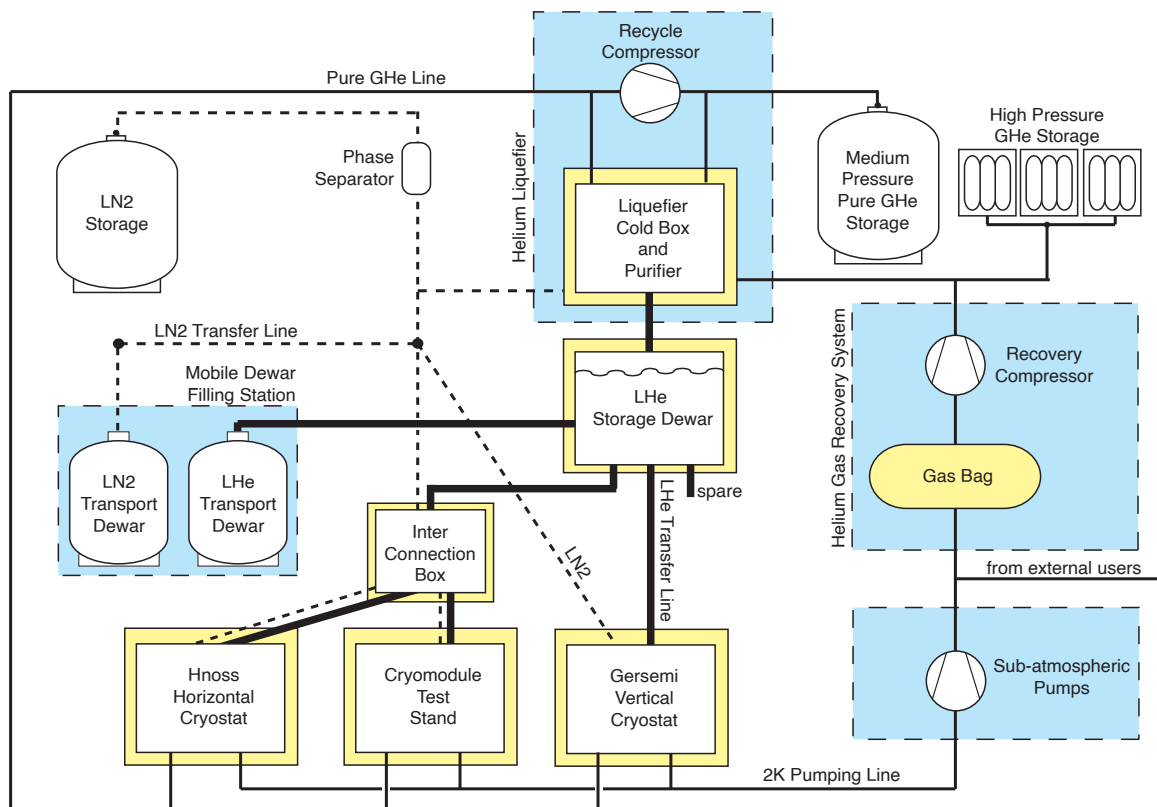


Figure 7: Schematic view of the cryogenic system showing the helium liquefier (top centre) delivering liquid helium via the storage dewar either to the interconnection box, and to Hnoss (figure 2 and 3) and the cryomodule (figure 4), or to Gersemi (figure 5 and 6). The sub-atmospheric pumps (bottom right) facilitate operation at 2 K. Liquid helium and gas helium connections are shown as solid lines and liquid nitrogen as dashed lines.

Table 1: Main parameters of the cryogenic system.

Liquefier	
- nominal capacity	140l/h at 1.15 bar 150l/h at 1.23 bar
- pre-cooling	70l/h liquid nitrogen
- purifier minimum inlet pressure	25 bar
Liquid helium storage dewar	2000l
Recovery gas balloon	100 m ³
Recovery compressors	>75 m ³ /h at 200 bar
High pressure storage	14.4 m ³ at 200 bar
Sub-atmospheric pumps	3.2 g/s at 10 mbar 4.3 g/s at 15 mbar

To avoid clogging of the cold box by frozen impurities during long-term operation, it is equipped with adsorbers that freeze out impurities at 80 K and 20 K. To prevent warming-up the whole cold box to regenerate the 80 K adsorber, it is equipped with valves for in-line regeneration.

The 2000l storage dewar acts as a buffer in case a different liquid helium throughput rate is required than provided by the liquefier cold box. The control software can adjust the liquefaction rate to maintain a constant liquid level in the storage dewar by adjusting the gas pressure at the inlet of the cold box. The storage dewar has four connections for the distribution of liquid helium. One is used to fill mobile dewars and the other three have integrated cryogenic valves, one of which links to the interconnection box (and from there to Hnoss and the cryomodule test stand), another links to Gersemi, while the last is a spare.

The helium gas returning from the cryostats and external users is fed back to the recycle compressor. A medium pressure tank serves as buffer for the pure gas helium in case the incoming flow to the recycle compressor is higher than required by the cold box. If more gas is needed, it can be provided from a high pressure gas storage. Before being used, this gas is sent through a freeze-out purifier included in the liquefier cold box to remove any impurities.

3.2 Sub-atmospheric Pumping

The sub-atmospheric pumping system is used to lower the pressure of the liquid helium bath in the cryostats and thereby the temperature. The dominant constraint for the minimum temperature is the pressure that can be reached by the pumps, which in turn depends on the return mass flow at the lowest pressure. The system has a flow capacity of 10 g/s at 200 mbar down to 3.2 g/s at 10 mbar (room temperature). Assuming that the flow capacity is roughly proportional to the pressure, the system supports a flow of 4 g/s at 31 mbar which corresponds to about 100 W cooling power at 2.0 K.

The pumping system is an integrated set of roots and dry-pumps. The first stage consists of two roots pumps in parallel, the second stage consists of a single roots pump, and the third stage consists of two dry roughing pump sets connected in parallel. Water cooled heat exchangers refrigerate the gas between the stages. Pressure regulation is achieved either by regulating the speed of the pumps or controlled opening of a butterfly valve between pumps and liquid helium bath.

The helium gas from the sub-atmospheric pumping system is recovered in a 100 m³ balloon at atmospheric pressure. The same gas balloon is also fed with helium gas recovered from colleagues using mobile dewars in adjacent faculty buildings up to 1 km distance (marked as “from external users” in figure 7). The gas balloon is emptied by a set of recovery compressors that link to the high pressure gas storage and then to the freeze-out purifier inside the liquefier cold box before being reused. The total amount of helium in the system is monitored in order to track losses [20].

Table 2: Main parameters of the tetrode RF stations.

Frequency	352.21 MHz
Bandwidth at 3 dB	>250 kHz
Repetition rate	14 Hz
RF Pulse length	3.5 ms
Maximum peak output power	400 kW
RF Output connection	6-1/8 inch, coaxial, 50 Ω
Cooling	water (anode) and air (filament)

4 Radio-Frequency Powering System

FREIA developed two prototype RF stations for testing ESS double-spoke cavities at 400 kW, 352 MHz, and corresponding RF distribution. R&D work is ongoing for the development of solid-state amplifier technology.

4.1 RF Power Stations

The RF power stations were developed as prototype for the ESS. The design was made in 2012 and combines two tetrode amplifiers for an output power of 400 kW pulsed at 14 Hz [21]. The main parameters are listed in table 2 and the schematic of the tetrode based RF power station design is shown in figure 8. The low-power RF input from a signal generator enters from the left. A hybrid

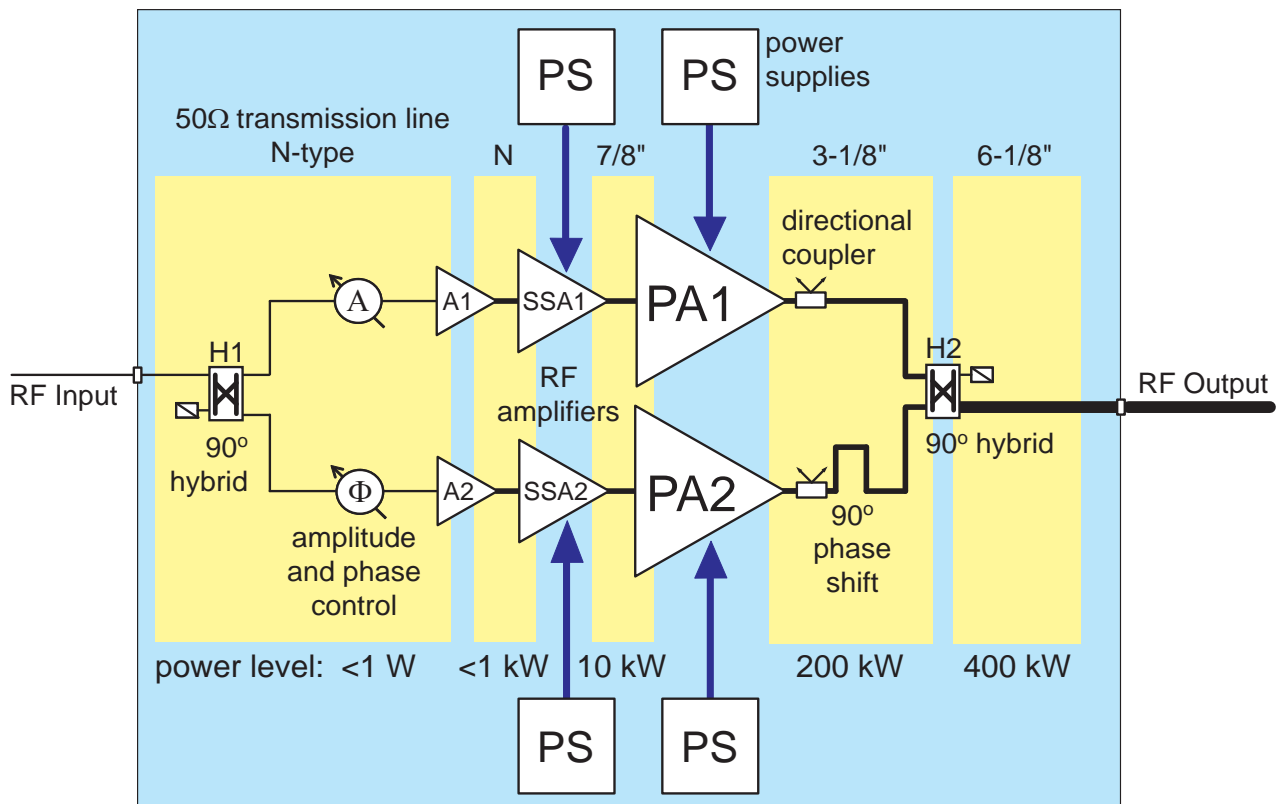


Figure 8: Schematic of the RF power station showing the RF signal input (left), split in two paths leading via two pre-amplifier stages (A1, A2, SSA1, SSA2) to the tetrode amplifiers (PA1, PA2). Power levels, phase differences, coaxial connection types and other ancillary components are indicated.

splitter (H1) divides this low-power RF signal into two equal-amplitude signals with a 90° phase difference which each pass through individual amplification channels. One of the signal channels incorporates amplitude regulation and the other phase regulation to balance the signal amplitude and phase at the output of the amplifier chains. Then the signals pass through solid-state amplifiers A1 and A2 followed by amplifiers SSA1 and SSA2 [22]. The combined amplification of these solid-state amplifiers is in the order of 70 dB reaching a signal level around 10 kW. This signal then enters the final amplification stage, the tetrode amplifiers PA1 and PA2. These have a minimum gain of 13 dB, a conservative estimate as it is expected that the amplification gain of the tetrodes deteriorates with ageing. After the amplifiers, the 90° phase difference due to the input splitter H1 is compensated in order to match the phases of both signals in the hybrid combiner H2 producing the output signal. The hybrid combiner has a 0.15 dB loss so the total amplification of the system is about 80 dB and a RF output signal in the order of 400 kW is achieved.

Both signal channels contain several directional couplers for monitoring the signal phase and amplitude. As the power levels in the amplifier chain gradually increase, the size of the transmission line increase from N-type coaxial cables to 7/8 inch coaxial line at the output of the solid-state amplifiers, to 3-1/8 inch at the output of the tetrode tube amplifiers, and finally 6-1/8 inch after the hybrid combiner. The tetrode amplifiers are protected from reflected power by a circulator at the RF output which is not part of the RF power station itself.

Each tetrode tube has four power supplies: one for the filament, screen grid, control grid, and

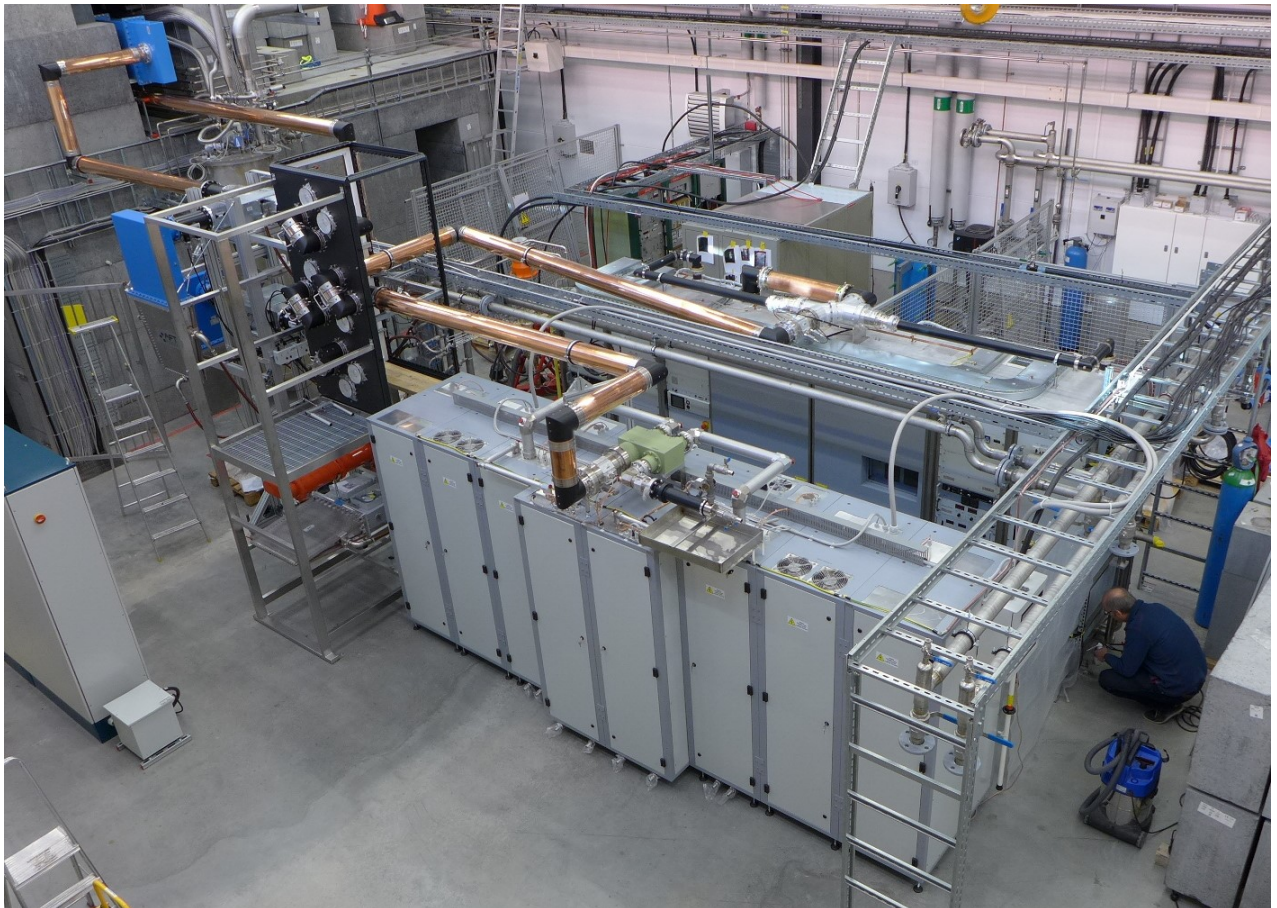


Figure 9: Photo with the two tetrode based RF stations (gray 8-door racks) in the centre and the bunker on the left. Coaxial RF transmission lines (copper coloured) come out from the top of the RF stations and go to the switch panel (black) from where they are routed to the bunker. One coaxial line enters directly and the other is connected to a (blue) waveguide transmission line.

anode respectively. The anode power supply is a high voltage power supply providing a voltage up to 18 kV based on a capacitor bank and charging unit [21]. The high voltage anode power supply is protected against short circuit by a crowbar and in one of the RF stations also by a series switch circuit. The control grid power supply is pulsed between two values: one for nominal operation of the tube and one for blocking the anode current in-between RF pulses which increases the energy efficiency.

An initial survey revealed that the most suitable tetrode tube available was the TH595 [23]. It can operate at power levels up to 200 kW in pulsed mode with a gain of 15 dB and an efficiency of 65%. This tube has a water-cooled anode and air-cooled cavity and tetrode connector, and can sustain an anode dissipation up to 40 kW continuous operation. It is used with a 352 MHz output cavity named TH18595A. Recently an improved tetrode tube version TH595A has become available with a new screen-grid design allowing a higher heat load and thereby enabling a possible higher duty cycle under ESS specification in case of a future power upgrade of the ESS. Thermal cycling effects due to switch-on and switch-off decrease the life time of the tube. Therefore, a “dark heating” operation mode is used during long periods of standby time in which the filament voltage is decreased substantially while avoiding a full thermal cycling of the filament.

Two tetrode RF stations based on our design were ordered from industry. The initial design of the first RF power station was adapted for the second RF power station adding an option for continuous operation and pulsed operation at 28 Hz repetition rate. A separate solid-state pre-amplifier was included for the continuous operation in parallel to the pulsed-mode pre-amplifiers. The two RF power stations, shown as the two 8-door racks in the center of figure 9 were installed at FREIA in 2015 and 2016 respectively and have been in operation since then [24, 25]. Based on this development, ESS chose a similar layout for their spoke RF power stations.

4.2 RF Power Distribution

The peak and average power levels for the 352 MHz RF power stations are such that coaxial transmission lines can be used, visible as the copper tubes on top of the RF stations in figure 9. These are 6-1/8 inch coaxial lines as compared to more bulkier 23 inch wide (half-height WR2300) waveguide transmission lines chosen for example for the ESS accelerator tunnel [26]. A coaxial circulator for 400 kW peak power was prototyped and is now also used at ESS.

Having several RF power stations, connected to multiple locations, demands a flexible solution for the RF power distribution. This was solved by connecting the 6-1/8 inch coaxial transmission lines from the RF power stations to a manual switch panel with 3 inputs, 4 outputs. The switch panel has 8 internal connectors which allows any possible input-to-output combination using fixed-length U-shaped coaxial-line connectors together with 4 permanent interconnections. As shown in figure 10, the four outputs of the main switch panel (marked switch #1) can be connected to either a load, cavity, or other test location. A circulator is installed on each connection to a test location. The outputs to a load are used when testing and tuning the RF power stations. Two smaller switch panels (marked switch #2 and #3) increase the switching options. The switch panels are equipped with interlocks so the control system can monitor the switch positions.

The ESS double-spoke cavities are equipped with a WR2300 half-height waveguide transmission line as input. Therefore coaxial-to-waveguide transition are installed in the final few meters before the cavity. The RF distribution system is equipped with directional couplers to monitor forward and reflected power levels.

4.3 Solid-state Amplifier Development

The possibilities of solid-state transistors for use in high-power RF amplifiers, as demonstrated at SOLEIL and other accelerators [27, 28], encouraged the development of technology demonstrating parts for an ESS type RF power station to replace the tetrode amplifiers described above. It was

decided to concentrate on the two of the technologically important parts: the transistor amplifier module and the RF power combiner.

A single transistor version was chosen for the amplifier module, optimized for overall efficiency and ease of manufacturing. The design effort resulted in a single-ended amplifier at 352 MHz realized in a planar printed circuit board technology and avoiding using complex circuits, such as baluns, while offering the possibility to make all components machine mountable. An output power of 1.3 kW at 71% efficiency and 19 dB gain was achieved while operating with ESS parameters [29].

An eight-transistor based technology demonstrator was constructed and operated successfully with feedback compensation for an optimized output pulse stability [30, 31]. To reduce losses, the output of each transistors is tuned within 0.5 dB gain and 5° phase. A total output power of 10.5 kW was achieved as shown in figure 11. Proportional and integral loop controllers, with a 6 μ s processing time, compensate the droop of the RF output power within the pulse caused by the capacitor bank powering the transistors. The variation of the uncompensated power amplitude is on the order of 1 kW, while the compensated variation over the pulse is only 20 W, which is equivalent to 0.2% [31]. No instabilities appeared during 4 h test runs while the temperature stabilized at the transistor and combiner [32]. For a multi-hundred kW RF station, the RF output of several 10 kW amplifier stages can be combined by a 12-ports 100 kW re-entrant cavity type combiner which can feed directly into a waveguide connecting the RF station to the accelerator cavity [33, 34].

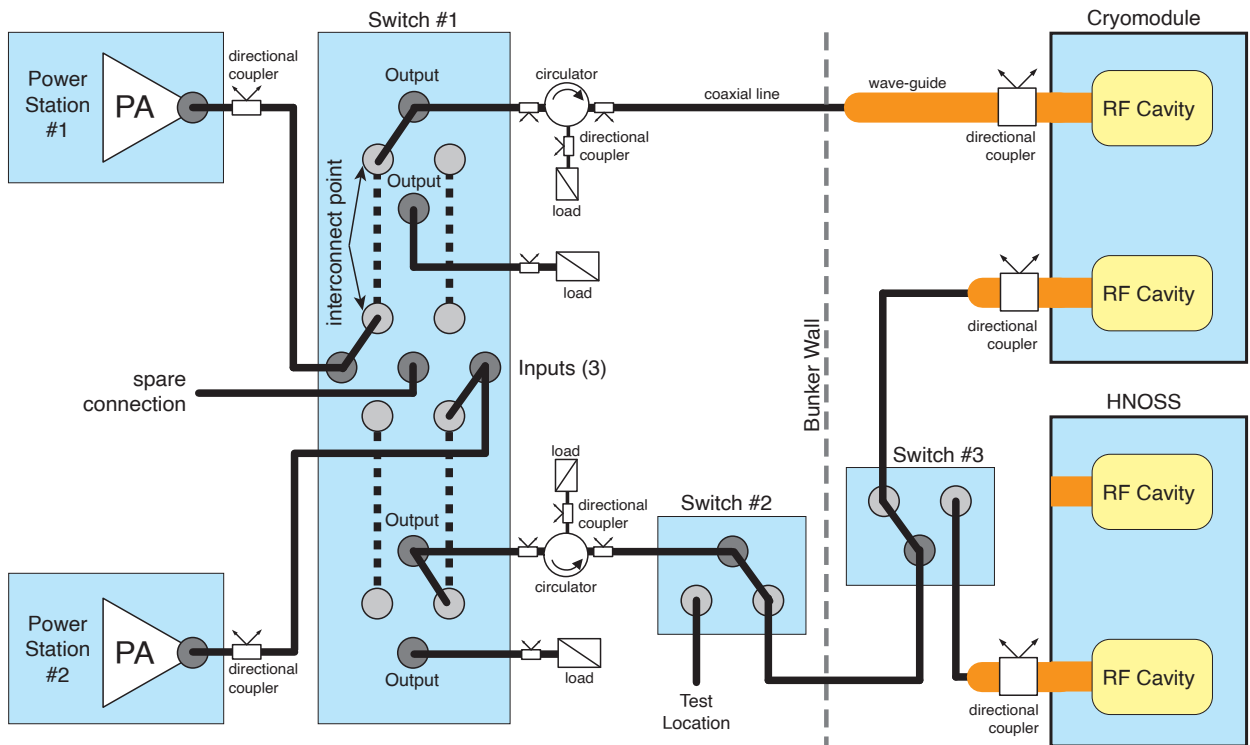


Figure 10: Layout of the RF distribution from the top of the RF power stations (also shown in figure 9) through coaxial lines to the switch panel and further on to the bunker either via coaxial lines (black) or waveguides (orange).

5 Test Infrastructure

A key part of the test infrastructure is the control system. This includes slow controls, monitoring of the infrastructure and equipment, and the fast controls of RF power regulation and measurement, sometimes also called the Low Level RF system (LLRF). In addition there are interlock systems for the protection of the superconducting cavities and magnets to be tested, as well as for the personnel safety.

5.1 Slow Control and Interlocks

The slow control system at FREIA is based on EPICS (Experimental Physics and Industrial Control System) [35] and LabVIEW [36]. The EPICS software is widely used at research institutes for the control of accelerators. EPICS is a distributed system consisting of a number of so-called Input/Output Controllers usually equipped with hardware interfaces to the controlled process, computers running services like archiving, logging, alarm, and computers used as operator consoles. All these units are interconnected using an ethernet network.

The EPICS based controls are used at the top level to provide the operator with a common interface to connect together different systems which might have their individual proprietary control system. This includes systems based on commercial industrial programmable logic controllers (PLC) or home-built laboratory systems based e.g. on Raspberry Pi hardware [20].

The LabVIEW based controls are typically used for more complex experiments and control programs. The LabVIEW controls are used for the conditioning and testing of superconducting cavities and cryomodules. These methods and procedures are often modified for specific experiments to adjust to changing and evolving requirements from the end-user.

5.2 RF Controls

At FREIA, the LLRF system has been developed based on National Instruments PXI-type hardware including so-called field-programmable gate arrays (FPGA) for fast data processing. To operate the cavity, either one locks the resonance frequency of the cavity, so the RF power station can be locked to the same frequency, or the RF power station follows the changing resonance frequency of the

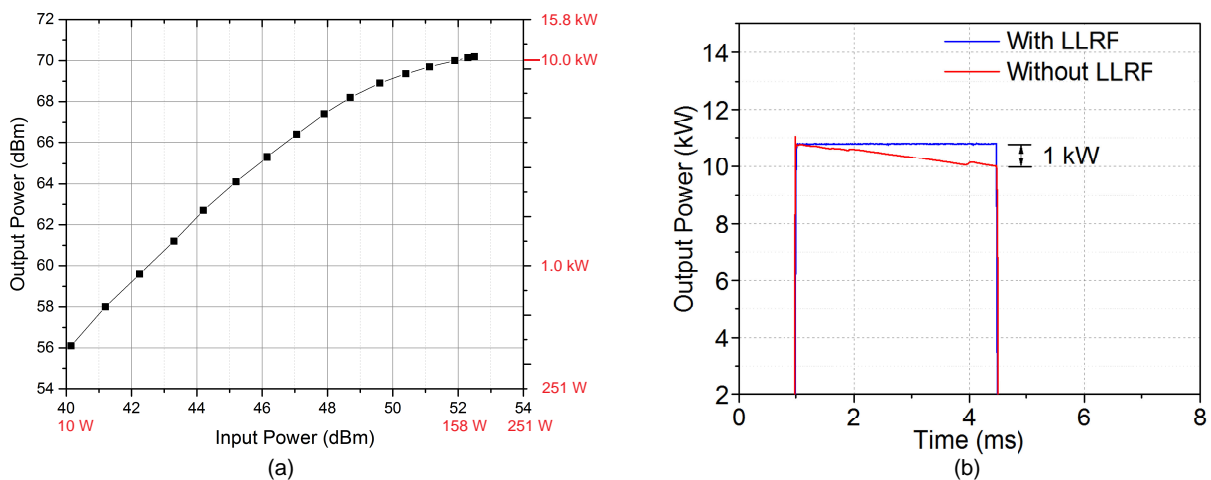


Figure 11: Performance of the 8 transistor technology demonstrator. (a) Output power as function of the input power in logarithmic scale. Maximum output 10.5 kW (70.2 dBm) at 0.178 kW (52.2 dBm) input. (b) Variation of the uncompensated power amplitude during the pulse is in the order of 1 kW, while the compensated variation is only 20 W at 10 kW output power.

cavity [37, 38]. The first operation mode is achieved with a generator driven loop and the second with a phase-locked loop or a self-excited loop.

In the signal generator-driven loop, the cavity resonance frequency is locked and a signal generator produces an RF signal with a fixed frequency, which is then amplified by the RF power station and sent to the cavity. A signal proportional to the accelerating field in the cavity is picked up by an antenna in the cavity and then used by the control system to tune cavity phase and field amplitude.

In the self-excited loop [39, 40], a free-running RF amplifier drives a high-gain positive feedback loop that is by nature unstable and operates at a limit cycle defined by the cavity that functions as a narrow bandpass filter. The loop follows changes in the cavity's resonance frequency and therefore there is no need for an external frequency source and frequency tracking feedback. The self-excited loop developed at FREIA has a maximum gain of up to 100 dB and is operated with either an analogue trombone-type phase shifter or a digital phase shifter. A diagram of the self-excited loop is shown in figure 12. Before entering the phase shifter, the pick-up signal from the cavity passes through an amplitude limiter and amplifier to ensure an adequate signal amplitude level. After the phase shifter, the signal passes through a bandpass filter selecting the main loop frequency after which the signal is amplified and sent to the RF power station and back into the cavity. If we do not want to operate the loop in continuous wave, the signal pulse length in the loop can be controlled by a switch. Circulators are included throughout the loop to protect amplifiers from reflected signals. An interlock switch is available to turn off the loop.

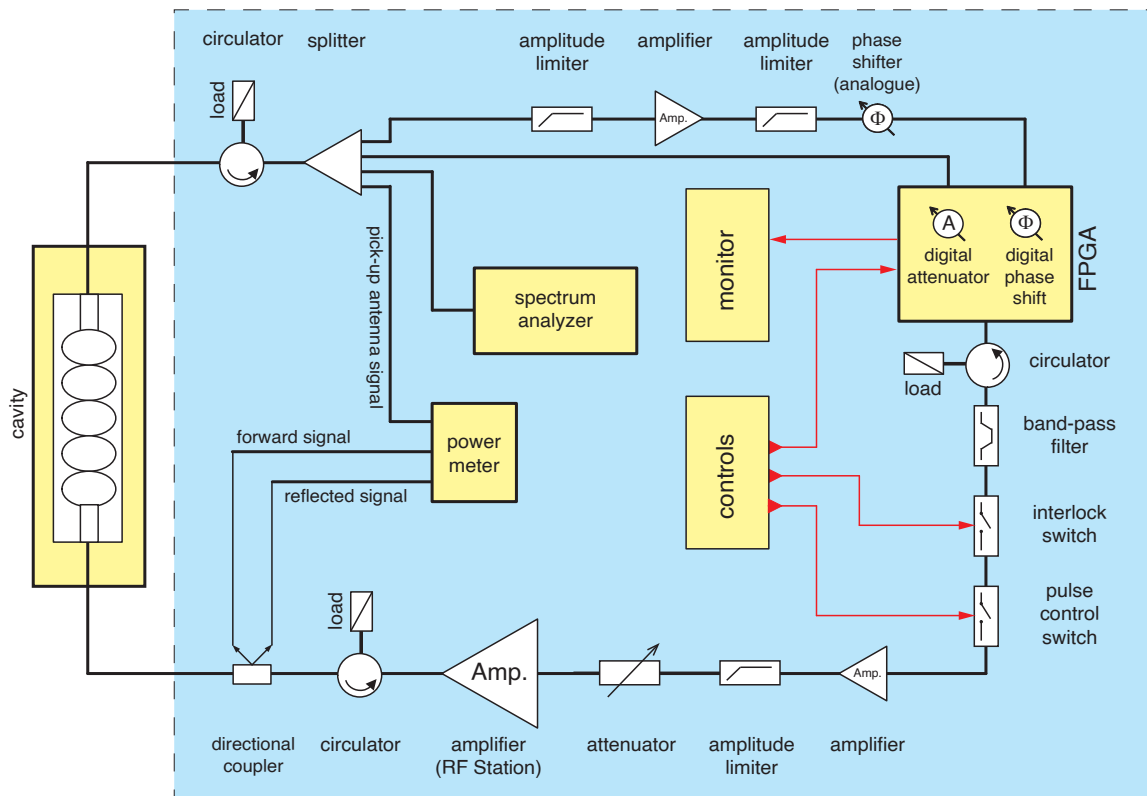


Figure 12: Diagram of the self-excited loop. The signal from the cavity antenna (top left) passes through signal preparation components to the analogue phase shifter and digital phase shifter (top right) before passing through additional filters and amplifiers back to the cavity. The performance of the loop is mainly monitored in a time domain window and a frequency domain window in a computer connected to the FPGA unit, with in addition a spectrum analyzer and power meter.

A quench detection algorithm is integrated into the digital RF control system that regulates the signal generator-driven and self-excited loop. This is especially of importance for the self-excited loop as during a cavity quench, the cavity's resonance frequency changes and the self-excited loop will follow the drift in frequency and keep powering the cavity. The algorithm constantly monitors the loaded-Q value of the cavity. In pulsed operation of the loop, the FPGA, that processes the data from the loop, calculates the slope of the RF field decay at the end of each pulse. If the exponential time constant, which is equal to the inverse of the decay rate, is smaller than a pre-calculated or measured value, it is assumed that a quench is starting to develop in the cavity. In this case, the control system will engage an interlock to interrupt the RF signal to the cavity.

6 Recent Results

Several cavities and cryomodules were tested at the FREIA Laboratory. Cavities tested in Hnoss were fitted with a jacket serving as liquid helium vessel. The first two cavities, a single-spoke and a double-spoke, were tested with an input power in the order of 100 W, which we call low-power tests. The next two cavities, a double-spoke and an elliptical, were tested at an input power above 100 kW, which we call high-power tests. The Gersemi vertical cryostat has been used for testing a crab cavity without a liquid helium vessel.

6.1 Single-spoke Cavity Low-power Test

The first cavity test in Hnoss was a low-power test of a single-spoke cavity borrowed from IJCLab. It was used to commission the cooling and test methods including the used hardware set-up such as controls and self-excited loop. The first step was to understand and develop appropriate calibration procedures required as an important step for any accurate measurement [41]. For example, as the attenuation of the copper cables for RF measurements depends on their temperature, all calibrations had to be performed after cool-down of the cavity to its 2 K operating temperature [42]. The cable calibration was performed using a vector network analyzer and RF power meters. Then, using the self-excited loop, it was possible to proceed making accurate measurements of the cavity's resonance frequency, Q-factor, and accelerating gradient. Based on the test results, verified with previous test results from IJCLab, we developed an automatic test interface to improve the test efficiency and could, for example, shorten the Q measurement from two days to twenty minutes.

6.2 Double-spoke Cavity Low-power Test

The second test in Hnoss was a low-power test of a 352 MHz double-spoke cavity, also from IJCLab, which was used to test the self-excited loop [44]. A high-precision Q-surface method was developed to accurately measure the Q_0 quality factor of the cavity as function of the cavity voltage or accelerating gradient [45]. Typical uncertainty of the Q_0 factor found in this way is in the order of 10 to 15%. The standard Q-factor measurement suffers from a deficiency originating from a single data point measurement of the reflection coefficient. With a Q-surface method, we are able to improve the accuracy by an order of magnitude. In order to obtain the Q-surface, for fixed forward power to the cavity we change step-by-step the phase shift across the cavity by tuning the digital phase shifter installed in the self-excited loop. This procedure is performed for each power level of interest, yielding the complex reflection coefficient of the cavity as a function of the cavity voltage and phase shift as shown in figure 13. The measurement points are grouped into slices around the same cavity voltage value, with each slice of measurement points forming a circle in the two dimensional space of the complex reflection coefficient. An accurate calculation of Q_0 is then obtained from the circle radius by means of a least-square minimization.

6.3 Double-spoke Cavity High-power Test

The third test in Hnoss was the first one using the high-power RF stations. The double-spoke cavity, equal in design to the previous cavity tested at low-power, was equipped with liquid helium jacket, high-power RF input coupler, and frequency tuning system. As such it was a completely equipped prototype for the ESS accelerator [46]. Figure 14 shows a photo of its installation in Hnoss.

The RF input-coupler was conditioned at room temperature and then twice at cryogenic temperature (cavity at 2 K). The first cold conditioning was done with an LLRF system borrowed from IJCLab. The second cold conditioning was done with the FREIA LLRF system. The RF station power level is controlled by the automatic conditioning software, while all essential safety interlocks are implemented in hardware.

RF power conditioning is done in standing wave mode with pulse length increasing from 20 to 2860 μs . During each step of selected pulse length, the power ramps up slowly in steps depending on various parameters set in the software until the maximum defined RF power is reached. Two

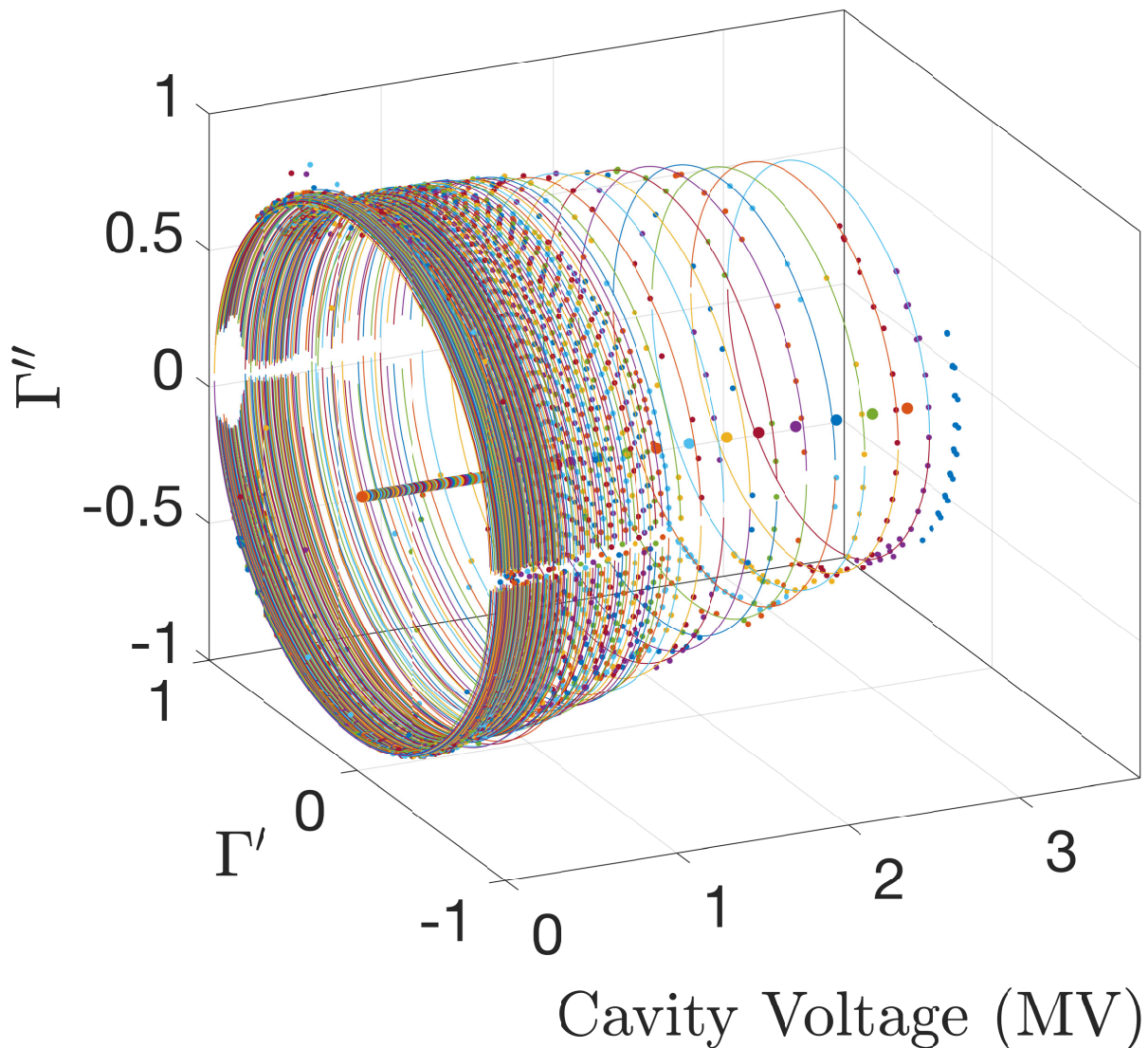


Figure 13: Q surface plot with the measured real and imaginary parts of the reflection coefficient versus cavity voltage [43]. The data points of the same color are obtained for fixed forward power to the cavity but different phase shifts through the self-excited loop. The circles are the guide to the eye for data points grouped into thin slices (Q-circles) having approximately the same cavity voltage.

software vacuum thresholds are used: as long as the vacuum pressure measured at the power coupler is below the first threshold, the RF power is step-wise increased. When the vacuum pressure rises above the first software threshold, the RF output power is kept stable until the vacuum pressure recovers. Otherwise, if the vacuum pressure increases above the second threshold, the RF power is decreased until the vacuum pressure decreases below the first threshold. The RF frequency used during the power coupler conditioning is just outside the resonance frequency of the cavity to avoid RF fields building up inside the cavity.

Next the cavity is conditioned using a pulsed self-excited loop mode. First, at very low power, a digital phase shifter is used to vary the loop delay, and thereby the frequency, around the cavity resonance frequency. This creates a controlled sweep of the field distribution back and forth along the coupler walls. In the second phase the RF power is ramped up while keeping a fixed pulse length. After about 30 hours of conditioning and passing through three major multipacting regions, the cavity package reached a stable 9 MV/m flat-top accelerating gradient. This is slightly above the nominal gradient for this cavity design intended to be used for the ESS accelerator [47].

6.4 Elliptical Cavity High-power Test

The fourth test was a high-power test of a prototype 704 MHz elliptical cavity for the ESS accelerator. The cavity was equipped with high-power RF input coupler and frequency tuning system. It was tested to verify design and operation of the high-power coupler. RF pulses with different amplitude, duration, and repetition rate recreate a similar situation as the cavity would experience in the accelerator. Overall, a similar test program was performed as for the high-power test of the double-

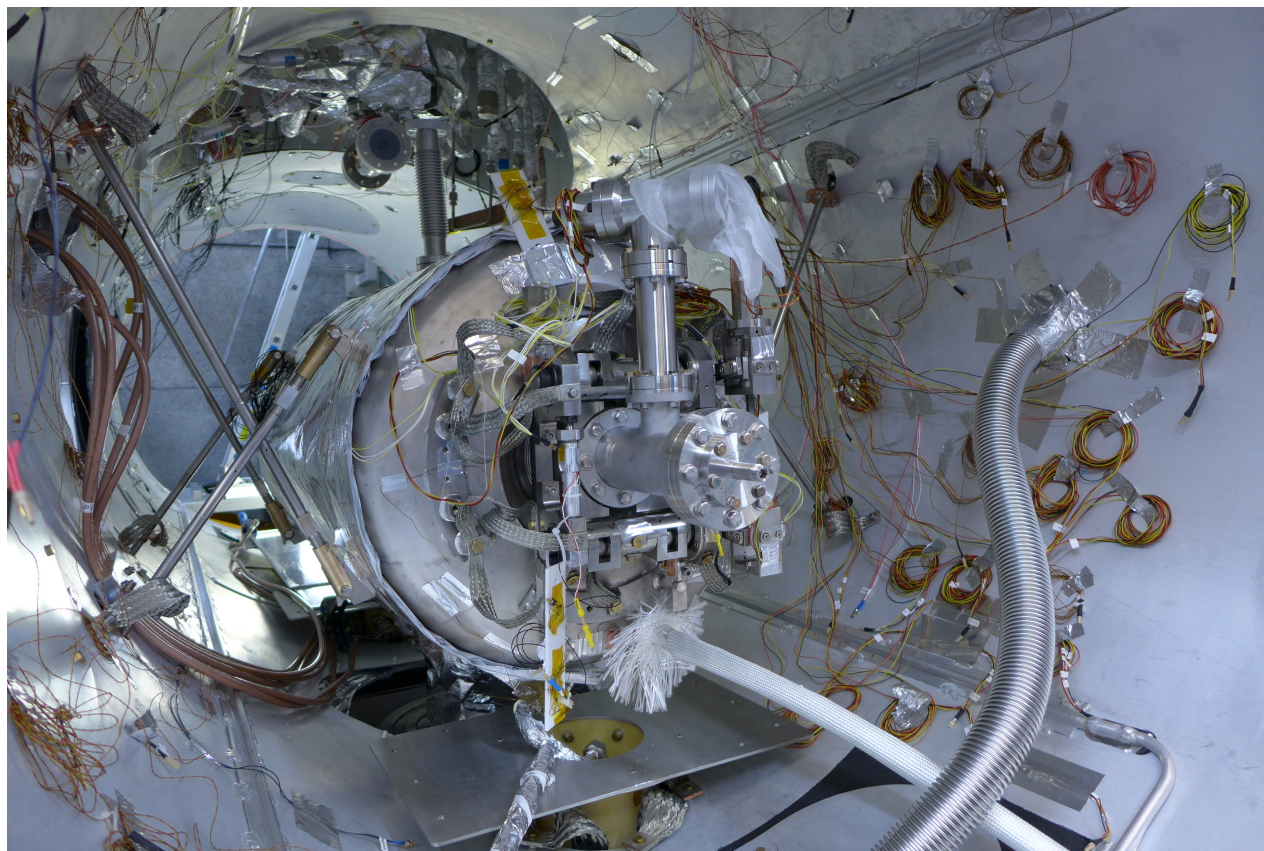


Figure 14: On-going installation of a double-spoke cavity in Hnoss, hanging from the vacuum vessel wall by support rods. The tuner is mounted at the near end and surrounds the beam pipe. Many signal cables are still taped to the inner wall of the thermal shield.

spoke cavity.

For this test we installed a 704 MHz klystron amplifier powered by a high-voltage pulse modulator, or modulator in short. We first commissioned the modulator followed by the klystron up to 1 MW peak power, limited by the RF load maximum power dissipation. The RF system and cavity conditioning was done with a LLRF control system developed by Lund University for use at the ESS accelerator, and with our own automatic conditioning system software.

The cavity was cooled down to 2 K two times without any significant issues. The power coupler and the cavity were successfully conditioned at high power RF. An accelerating gradient of 13 MV/m was measured with an incident peak RF power of 290 kW. Some outgassing and X-ray radiation occurred at intermediate field levels, but disappeared after a few hours of operation. The effect of the Lorentz force detuning was visible at high field, with a variation of the field amplitude on the flat top of the pulse [48, 49].

Two different methods are used for dynamic heat load measurements. The first method is by liquid helium evaporation, measured via a gas flowmeter placed after the sub-atmospheric pumps. The second method is by pressure rise, and is also used to cross check the system performance. The liquid helium volume of the cavity is closed off and the rise of helium pressure is measured as function of time. A heat load calibration curve was prepared by repeatedly measuring the relative rise of the pressure level caused by a known heat load from a resistive heater.

6.5 Spoke Cryomodule High-power Test

A prototype cryomodule for the ESS accelerator [50] equipped with two double-spoke cavities was tested in 2019 with more optimized parameters based on the lessons learned from the earlier tests

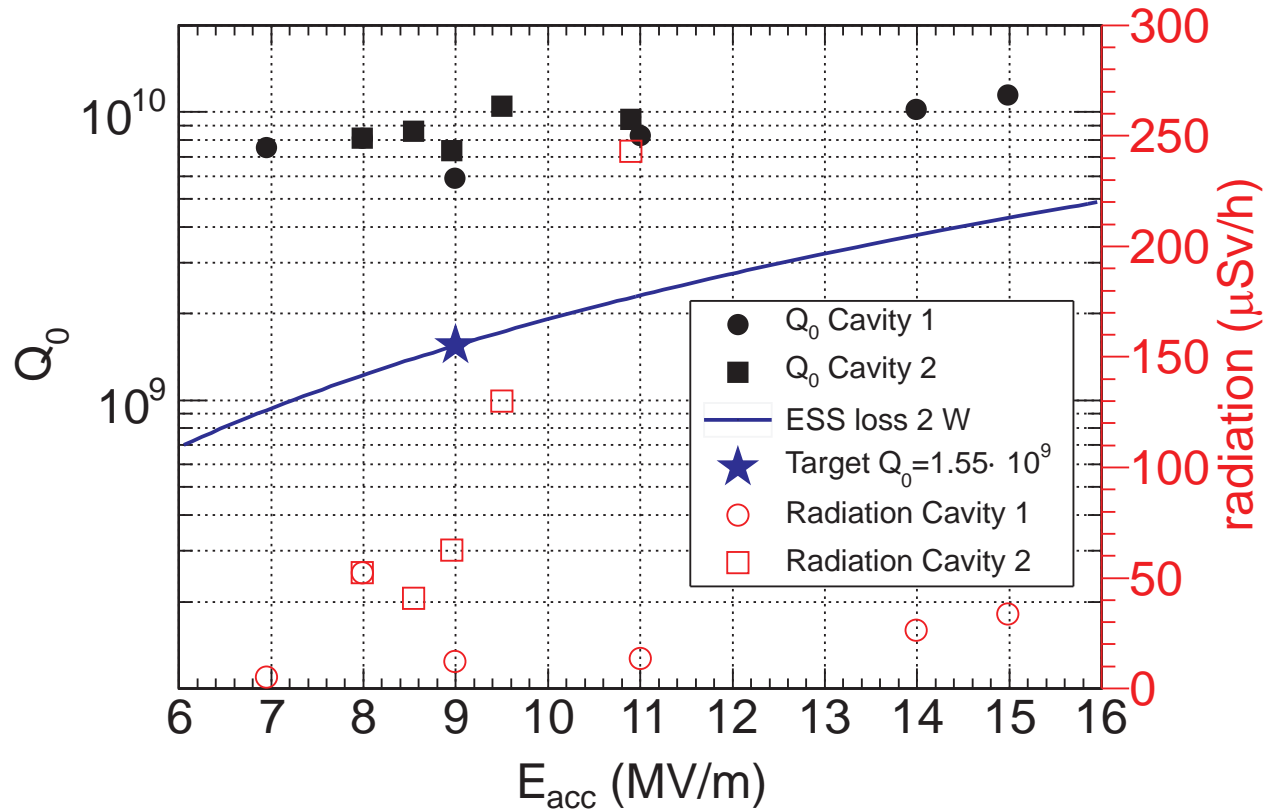


Figure 15: Measured Q factor of the two cavities in the prototype cryomodule. Data is compared to the ESS target value (star), measurements in a vertical cryostat before mounting in the cryomodule (courtesy IJCLab), and X-ray radiation levels recorded when performing the measurements.

described above. The test included studying the conditioning procedure, accelerating gradient, dynamic heat load, cold tuner, piezo actuator, diagnostics, RF controls, and safety interlocks. A special cryogenic valve box was installed next to Hnoss, in the same bunker, and connected in parallel onto the cryogenics distribution system using the same cryogenic interconnection box as for Hnoss.

The conditioning procedure was divided into power coupler conditioning and cavity conditioning [51]. First, the power couplers were conditioned at room temperature before the cooling of the cryomodule was started. Second, the power couplers were reconditioned after the cavities were cooled down. Finally, the cavities were conditioned. Every time a thermal cycle occurred, for example for dedicated tests of the cryogenic system, these three steps were repeated to recover the functionality of the cavities.

The cavity conditioning started in pulsed self-excited loop mode. A second conditioning of the cavities was performed with the generator-driven loop. The conditioning was carried out with 1 and 3.2 ms pulse lengths while slowly increasing the RF power and hence the accelerating gradient. Figure 15 shows the measured quality factor of both cavities as function of the accelerating gradient. Electron activities in the cavity were associated with X-ray dose rate and given only for a relative comparison of the level of radiation as function of the accelerating field. Both cavities in the cryomodule achieved the ESS nominal operation parameters.

The cryomodule was thermally cycled several times. Noticeable outgassing occurred every time the cavities warmed up above 20 K, with temperature and pressure ($<10^{-8}$ mbar) implying that nitrogen was the dominant vapour element. A small thermal cycle of the cavities from 2 to 50 K did not affect the conditioning. After a full thermal cycle to room temperature for one month, the re-conditioning of the couplers required only a few hours. However cavity re-conditioning took almost the same time as the first conditioning after the first cool down [52, 53].

6.6 Crab Cavity Low-power Test

A 400 MHz crab cavity prototype for the High Luminosity upgrade of the Large Hadron Collider (HL-LHC) was the first cavity tested in the Gersemi vertical cryostat. This cavity was a double quarter wave type for horizontal bunch crossing in the ATLAS detector of the LHC, operated in continuous mode [54]. The cavity was manufactured in the USA and previously tested at Jefferson Laboratory and CERN. The test in Gersemi was performed as a first step to validate the ability of FREIA to test these cavities and serve as a back-up test stand for CERN and the HL-LHC project. As the cavity came without its liquid helium jacket, it was tested in Gersemi with operation mode and insert type 1 (figure 6) and supported by a solid mechanical frame. Figure 16 shows the insertion of the cavity into Gersemi.

The cavity has been validated to operate above the nominal gradient of 3.4 MV at 2 K. Figure 17 shows the measured cavity Q factor versus the transverse RF voltage V_t . The cavity was also measured at 1.8 K to demonstrate the availability of Gersemi at both temperatures. The main challenge for the measurement was the high Lorentz force detuning of the cavity which shifted the resonance frequency as RF power levels increased. The experiment was not performed with a self-excited loop but with a phase-locked loop based on electronics lent by CERN. Cavity resonance was lost at 4.6 MV transverse voltage, both at 2 K and 1.8 K, which we interpret as the quench limit [55].

7 Current and Future Activities

The different development projects and subsequent testing of superconducting cavities has prepared the FREIA Laboratory for a wide range of accelerator development activities. Some of them are briefly explained below.

7.1 ESS Spoke Cryomodules

At the time of writing, FREIA is testing a series of 13 spoke cryomodules for the ESS accelerator. Like the prototype spoke cryomodule, each cryomodule is equipped with two double-spoke cavities. The first cryomodule arrived at FREIA in October 2020 and testing was completed in December 2020. To keep the ESS high-level planning, each of the next cryomodules is to be tested within a tight schedule. Turn-over is expected to reach an average of six weeks per cryomodule. It takes about one and a half week for reception tests and installation, one week for warm RF conditioning of the power couplers of both cavities, then one and a half week for cool down, cold RF conditioning and cold testing, one and a half week for warm-up and removal, and a few more days to prepare for shipment.

7.2 LHC High Luminosity Upgrade

Key elements of the HL-LHC project at CERN are superconducting magnets and cavities. FREIA is ideally suited to contribute to the development of such equipment. Work is ongoing in three areas: superconducting dipole magnets, superconducting crab cavities, and cryostats for the superconducting power link.

The Gersemi vertical cryostat is available both for superconducting magnet and cavity testing. The superconducting crab cavities are similar in design to the previously tested 400 MHz crab cavity. They are tested before mounting their liquid helium jacket and the test can therefore be performed in a simple liquid helium bath. The HL-LHC project is also interested in cold power testing of some 20 superconducting dipole magnets used for beam orbit correction. These magnets combine two dipole magnets, horizontal and vertical field direction, in a single device with each having a dipole

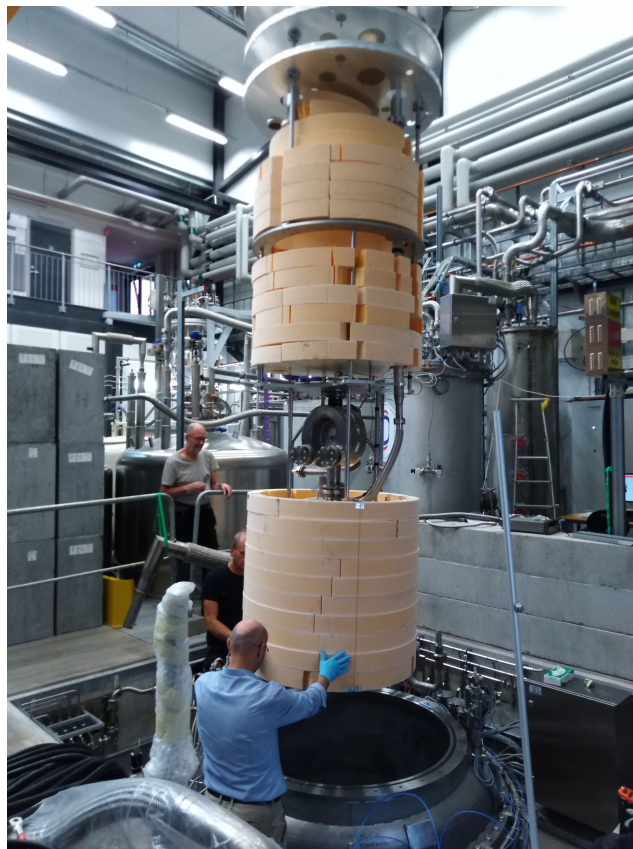


Figure 16: Lowering the insert with an HL-LHC crab cavity into Gersemi. Note the orange coloured foam to decrease the amount of liquid helium required to fill the large cryostat volume.

field strength of up to 2.2 T in different configurations with a length of either 1.5 or 2.1 m.

The HL-LHC includes a superconducting link which has to ensure a current-carrying capacity of up to 100 kA over a distance of 100 m [56]. This superconducting link connects several superconducting magnets to their respective power supplies by means of a vapour cooled superconducting cable. FREIA, in collaboration with CERN and Swedish industry, contributes to the construction of the cryostats that integrate and ensure cryogenic cooling with helium vapour of resistive splices between MgB₂ and BSCCO type superconducting cables.

7.3 Superconducting Canted-cosine-theta Magnet

In collaboration with Swedish industry, FREIA is developing a superconducting dipole magnet based on a canted-cosine-theta (CCT) layout, sometimes referred to as double-helix or tilted coils. The CCT design is based on two concentric modulated helical coils having a winding shift of π and inverse currents [57]. Advances in the accuracy of 3D machining technology have now made it possible to manufacture this kind of magnet layout by machining an accurate groove in an aluminium former [58]. Our CCT magnet is a dipole magnet build by the superposition of two oppositely skewed solenoids with respect to the bore axis. A 50 cm model dipole magnet, shown in figure 18, was fabricated and

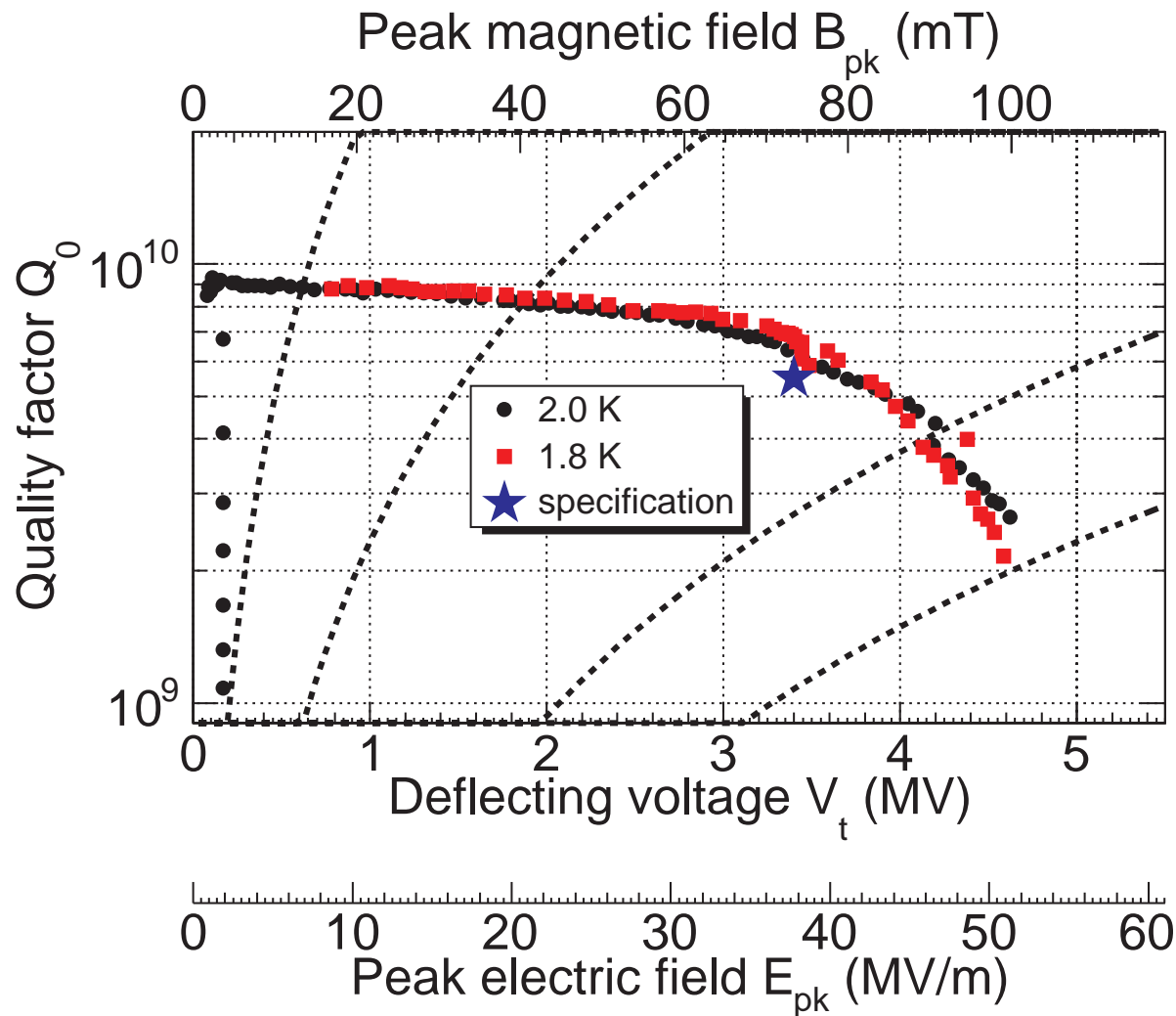


Figure 17: Measured quality-factor Q versus transverse voltage V_t for the HL-LHC crab cavity prototype. The nominal specification value is indicated by a star. Dotted lines indicate RF power levels in the cavity.

is waiting to be tested in Gersemi. Next we will start construction of a 1 m long CCT type dipole magnet that shall fulfil the specifications for a LHC type orbit corrector dipole magnet.

7.4 Vacuum Breakdown and High-gradient Acceleration

From the earlier participation in the Two-Beam Test Stand experiments at CTF3 [4] evolved an interest to probe the limits of electric field gradients in accelerating cavities. We developed a spectrometer for the measurement of dark and breakdown currents that is being operated at the CLIC high-gradient test stands at CERN. By using tomographic image reconstruction it became possible to obtain the vacuum breakdown location inside an accelerating structure [59].

Recently, we have constructed a cryogenic, pulsed, high-voltage system integrated in a stand-alone cryocooler to investigate the fundamental mechanisms of field emission and breakdown nucleation. In the system, high-field measurements can be carried out at ambient and down to cryogenic temperatures. The first results reveal a significant increase in the field holding capability of the copper electrodes when cooled and conditioned at cryogenic temperatures, between 30 and 90 K [60].

7.5 Lasers and X-ray Sources

Already before the establishment of the FREIA Laboratory, some of us were involved in the development of free-electron lasers (FEL). Noteworthy contributions are e.g. the Optical Replica Synthesizer for FLASH [5] and the Laser Heater for the European-XFEL [6]. We are now working actively on the design of soft X-ray FEL extension of the linac-injector at MAX IV [61, 62] and participate to the Eu-supported “XLS CompactLight” design study for a compact hard X-ray FEL facility [63]. The gained knowledge is being combined to develop a design for a compact electron and X-ray source at FREIA. The source would contain a normal conducting RF gun and superconducting accelerating cavities to provide 3 to 10 MeV electrons. At 3 MeV it can be used for electron diffraction measurements, and at 10 MeV to produce X-rays from Compton scattering.

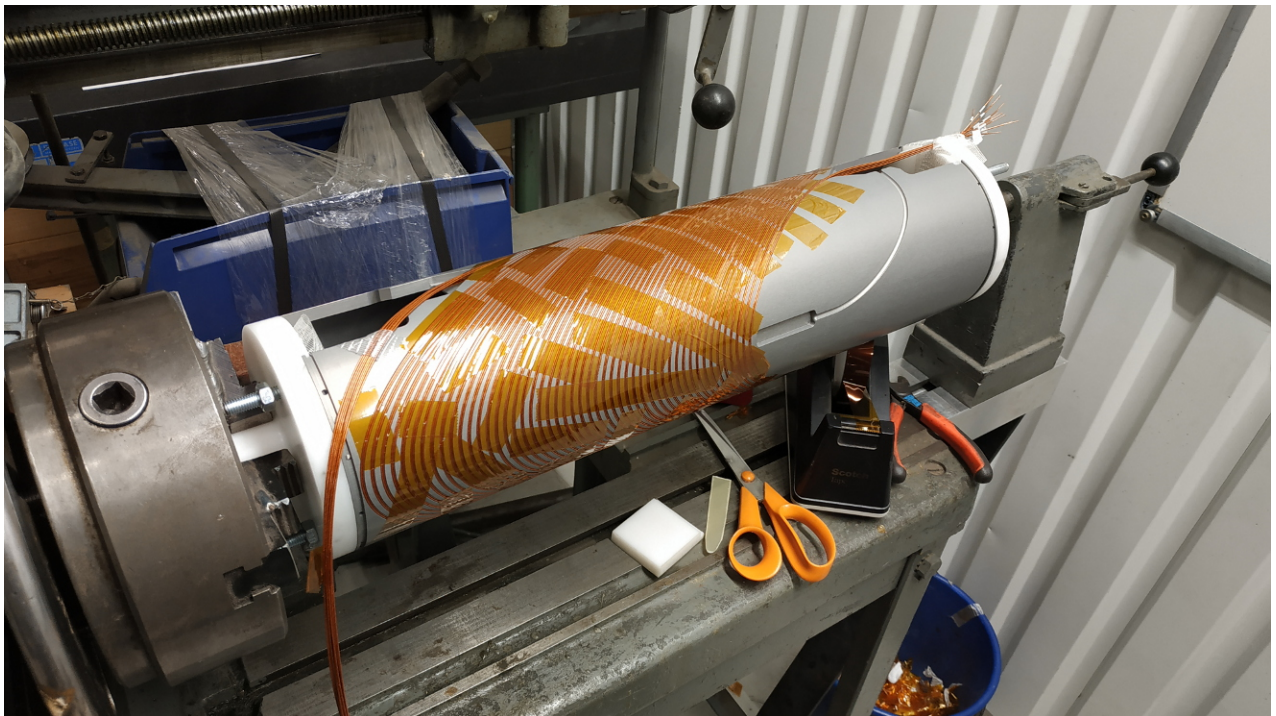


Figure 18: Winding a coil for the 50 cm long CCT model magnet. Photo courtesy Scanditronix Magnet AB.

7.6 Microwave Amplifiers and Communication

The work on the 352 MHz solid-state amplifier development has been extended to other frequencies and power levels. Designs and prototypes have been developed for power amplifier modules for cyclotrons in radioisotope production that operate in the low VHF band at 27 and 100 MHz [64, 65].

Research is ongoing on 60 GHz broadband antennas and transceiver chips for high-speed communication and data transfer in particle physics experiments. The upgrade of the Large Hadron Collider for high luminosity will result in multiple times higher event rates, which demands high data rate readout systems in the order of 50 to 100 Tbps. The feasibility of 60 GHz wireless links in harsh detector environments was studied by investigating different antenna arrays at 28 and 60 GHz and performance degradation of wireless communication chips after irradiation [66, 67].

7.7 Neutron Source

A commercial deuterium-tritium type neutron source is being procured by colleagues at the Department of Physics and Astronomy. The source will provide 14 MeV neutrons with a yield exceeding 10^{10} n/s. It will be used for academic and educational purposes, as well as industrial testing of radiation effects in electronics.

7.8 ESS Upgrade

The advent of the powerful ESS proton accelerator and the simultaneous interest in neutrino physics gave rise to the idea to use the ESS accelerator to generate, concurrently with the generation of spallation neutrons, an intense neutrino beam. The pulse repetition rate of the ESS accelerator will be doubled and every second pulse will be diverted to a second target station to produce a pion beam. The neutrinos from pion decay will be detected in a huge underground water Cherenkov detector ca. 500 km from ESS to study neutrino oscillations and leptonic CP violation. The muons from pion decay could also be accelerated and brought into collision to produce a very large number of Higgs bosons. ESSnuSB (ESS neutrinos Super Beam) [68] is a 4-years EU supported Design Study of this research program with scientists from FREIA working on the design of an accumulator ring needed to compress the 3 ms long ESS linac pulses to 1.3 μ s pulses.

7.9 Other International Projects

FREIA participates in the ARIES accelerator development project, a European wide project with 42 participating universities and institutes [69]. Our research on solid-state RF amplifiers is the FREIA part of the work package related to improving the sustainability and efficient energy management of accelerator infrastructures. The Hnoss and Gersemi cryostats and test infrastructures are shared as a trans-national access facility, which reinforced the case to construct the Gersemi cryostat for both superconducting cavity and magnet testing. Several of the cavity tests described above were performed in the framework of the ARIES trans-national access. Within the new European I.FAST project, FREIA will lead a work package to develop a RF amplifier around 750 MHz based on kW-level GaN transistors.

8 Conclusions

The FREIA Laboratory was initially conceived to develop part of the acceleration system of the ESS. From there it has developed into a versatile infrastructure to support the larger accelerator community by ensuring the performance of high-end components for future accelerators. One of FREIA's focal points is the test of superconducting RF cavities and magnets, which is facilitated by the availability of horizontal and vertical cryostats, cooled by liquid helium, and high-power RF amplifiers. The latter is a key component for the development of the power generation, distribution

and test of the spoke cavities for the ESS. In the past year, new fields of activity opened up with tests of HL-LHC crab cavities and magnets, and the development of canted-cosine-theta magnets. A second focal point is the development of solid-state power amplifiers and power combiners, which might well replace the RF vacuum-tube amplifiers that still power many accelerators today. These main fields of activity are complemented by other projects, such as the study of vacuum breakdown and the development of compact sources of radiation, which may expand in the future. Parts of the FREIA infrastructure are internationally accessible as trans-national access facilities, which is expected to widen FREIA's scope further.

9 Acknowledgements

We like to thank our colleagues at the FREIA Laboratory and Uppsala University for their support during this project. Our work would have been impossible to achieve without the support and advice from our colleagues at ACS Accelerators and Cryogenics Systems, CEA Saclay, CERN, the European Spallation Source ESS, IJCLab (former IPN Orsay), and Lund University.

This project has received funding from the Knut and Alice Wallenberg Foundation, the Vice-Chancellor and the Faculty of Science and Technology of Uppsala University, and the European Union's Horizon 2020 Research and Innovation programme under Grant Agreement No 730871, No. 777419, and No. 777431.

References

- [1] B. Hedin. Synchrocyclotron in Uppsala. *Kosmos (Stockholm)*, 30:144, 1952.
- [2] S. Holm et al. New Accelerators in Uppsala. *Physica*, 34:513, 1986.
- [3] Chr. Bargholtz et al. The WASA detector facility at CELSIUS. *Nucl. Instr. and Meth.*, A594:339, 2008.
- [4] R. Ruber et al. The CTF3 Two-beam Test Stand. *Nucl. Instr. and Meth.*, A 729:546, 2013.
- [5] G. Angelova et al. Observation of two-dimensional longitudinal-transverse correlations in an electron beam by laser-electron interactions. *Phys. Rev. ST Accel. Beams*, 11:070702, 2008.
- [6] M. Hamberg and V. Ziemann. Construction of the EU-XFEL Laser Heater. In *Proc. of the 37th Free Electron Laser Conference FEL15*, page 452. FEL 2015, August 2015, Daejeon, South Korea.
- [7] R. Ruber et al. An ultra-thin-walled superconducting solenoid for the CELSIUS/WASA experiments. *Nucl. Instr. and Meth.*, A503:431, 2003.
- [8] A. Yamamoto et al. The ATLAS Central Solenoid. *Nucl. Instr. and Meth.*, A584:53, 2008.
- [9] P. Clay et al. Cryogenic and Electrical Test Cryostat for Instrumented Superconductive RF Cavities (CHECHIA). *Adv. in Cryogenic Engineering*, 41:905, 1996.
- [10] H. Saugnac et al. Cryogenic Installation Status of the "CRYHOLAB" Test Facility. In *Proc. of the 10th Workshop on RF Superconductivity*, page 632. SRF 2001, September 2001, Tsukuba, Ibaraki, Japan.
- [11] W. Anders and J. Knobloch. Hobicat – A Horizontal Test Facility for Superconducting RF Cavities. In *Proc. 24th International Free Electron Laser Conference and the 9th FEL Users Workshop*, pages II–13. FEL 2002, Argonne, Illinois, U.S.A., September 9–13, 2002.

- [12] K.W. Shepard, M. Kedzie, J.R. Delayen, C. Piller, and A. M. Porcellato. Development of Niobium Spoke Cavities for a Superconducting Light-ion Linac. In *Proc. of the XIX International Linear Accelerator Conference*, page 956. LINAC 1998, August 1998, Chicago, Illinois, USA.
- [13] T. Junquera et al. Design of a New Horizontal Test Cryostat for SCRF Cavities at Uppsala University. In *Proc. of the 16th International Conference on RF Superconductivity*, page 328. SRF 2013, September 2013, Paris, France.
- [14] R. Santiago Kern et al. The HNOSS Horizontal Cryostat and the Helium Liquefaction Plant at FREIA. In *Proc. of the 5th International Particle Accelerator Conference* [70], page 2759.
- [15] N. R. Chevalier et al. Design of a horizontal test cryostat for superconducting RF cavities for the FREIA facility at Uppsala University. In *AIP Conf. Proc. 1573*, page 1277, 2014.
- [16] J. P. Thermeau et al. The First Tests on Vertical Cryostat Gersemi at FREIA Facility. In *Proc. of the 19th International Conference on RF Superconductivity*, page 923. SRF 2019, June-July 2019, Dresden, Germany.
- [17] V. Ziemann and R. Wedberg. Earth-field Compensation Coils for the Vertical Cryostat in FREIA. FREIA Report 2018/01, Uppsala University, 2018.
- [18] V. Ziemann et al. Retro-Fitting Earth-Field Compensation Coils to the Vertical Cryostat GERSEMI in FREIA. *Instruments*, 4 (1):8, 2020.
- [19] R. Ruber et al. The Cryogenic System at the FREIA Laboratory. FREIA Report 2015/03, Uppsala University, 2015.
- [20] V. Ziemann and L. Hermansson. Tracking the Helium Balance in FREIA. In *Proc. of the 7th International Particle Accelerator Conference*, page 1202. IPAC 2016, May 2016, Busan, Korea.
- [21] V.A. Goryashko et al. Proposal for Design and Test of a 352 MHz Spoke RF Source. FREIA Report 2012/04, Uppsala University, 2012.
- [22] R.A. Yogi et al. Uppsala High Power Test Stand for ESS Spoke Cavities. In *Proc. of the 26th International Linear Accelerator Conference*, page 711. LINAC 2012, September 2012, Tel Aviv, Israel.
- [23] R.A. Yogi et al. Selection of RF Power Source and Distribution Scheme at 352 MHz for Spoke Cavities at ESS and FREIA. FREIA Report 2012/01, Uppsala University, 2012.
- [24] M. Jobs et al. Itelco-Electrosys 400 kW RF Station Site Acceptance Test. FREIA Report 2015/07, Uppsala University, 2015.
- [25] M. Jobs et al. DB Science 400 kW RF Station Site Acceptance Test. FREIA Report 2017/01, Uppsala University, 2017.
- [26] R.A. Yogi et al. Design of the RF Distribution System for the ESS Spoke Linac. FREIA Report 2013/02, Uppsala University, 2013.
- [27] P. Marchand et al. High power 352 MHz solid state amplifiers developed at the Synchrotron SOLEIL. *Phys. Rev. ST Accel. Beams*, 10:112001, 2007.
- [28] P. Marchand. Review and Prospects of RF Solid State Power Amplifiers for Particle Accelerators. In *Proc. of the 8th International Particle Accelerator Conference* [71], page 2537.
- [29] D. Dancila et al. Solid-State Amplifier Development at FREIA. In *Proc. of the 5th International Particle Accelerator Conference* [70], page 2284.

- [30] D. Dancila et al. A Compact 10 kW Solid-State RF Power Amplifier at 352 MHz. In *Proc. of the 8th International Particle Accelerator Conference* [71], page 4292.
- [31] L. Hoang Duc et al. Feedback compensated 10 kW solid-state pulsed power amplifier at 352 MHz for particle accelerators. *Rev. of Scientific Instruments*, 90:104707, 2019.
- [32] M. Jobs et al. A 8-1 Single Stage 10 kW Planar Gysel Power Combiner at 352 MHz. *IEEE Trans. Components, Packaging and Manufacturing Technology*, 8 (5):851, 2018.
- [33] V. Goryashko et al. A megawatt class compact power combiner for solid-state amplifiers. *J. Electromagn. Waves Appl.*, 28 (18):2243, 2014.
- [34] V. Goryashko et al. 12-Way 100 kW Re-entrant Cavity-based Power Combiner with Doorknob Couplers. *IEEE Microw. and Wireless Compon. Lett.*, 28 (2):111, 2018.
- [35] Experimental Physics and Industrial Control System (EPICS). Project web page <https://epics-controls.org/>.
- [36] LabVIEW. Project web page <https://www.ni.com/labview>.
- [37] T. Powers. Theory and Practice of Cavity RF Test Systems. Thomas Jefferson National Accelerator Facility, 2007.
- [38] H.-D. Gräf. Experience with Control of Frequency, Amplitude and Phase. In *Proc. of the 5th Workshop on RF Superconductivity*, page 317. SRF 1991, August 1991, DESY, Germany.
- [39] J.R. Delayen. *Phase and amplitude stabilization of superconducting resonators*. PhD thesis, California Institute of Technology, Pasadena CA, USA, 1978.
- [40] J.R. Delayen. Self-excited Loop. Jefferson Laboratory LLRF Workshop, 25-27 April 2001, 2001.
- [41] H. Li et al. RF Test of the Hélène Single Spoke Cavity. FREIA Report 2015/10, Uppsala University, 2015.
- [42] H. Li et al. Calibration Procedure for RF Test. FREIA Report 2016/02, Uppsala University, 2016.
- [43] A.K. Bhattacharyya. *From Macroscopic to Microscopic Dynamics of Superconducting Cavities*. PhD thesis, Uppsala University, Uppsala, Sweden, 2018.
- [44] H. Li et al. RF Test of the ESS Double Spoke Cavity. FREIA Report 2016/01, Uppsala University, 2016.
- [45] V. Goryashko et al. A method for high-precision characterization of the Q-slope of superconducting RF cavities. *IEEE Trans. Microw. Theory Tech.*, 64 (11):3764, 2016.
- [46] H. Li et al. First High Power Test of the ESS Double Spoke Cavity. FREIA Report 10, Uppsala University, 2017/10.
- [47] H. Li et al. Characterization of a $\beta=0.5$ double spoke cavity with a fixed power coupler. *Nucl. Instr. and Meth., A* 927:63, 2019.
- [48] H. Li et al. First High Power Test of the ESS High Beta Elliptical Cavity Package. FREIA Report 2018/07, Uppsala University, 2018.
- [49] H. Li et al. First High Power Test of the ESS High Beta Elliptical Cavity. In *Proc. of the 29th International Linear Accelerator Conference*, page 841. LINAC 2018, September 2018, Beijing, China.

- [50] R. Garoby et al. The European Spallation Source Design. *Physica Scripta*, 93:014001, 2017.
- [51] A. Miyazaki et al. Contamination and conditioning of the prototype double spoke cryomodule for European Spallation Source. arXiv:2005.00761 [physics.acc-ph], 2020.
- [52] R. Santiago-Kern et al. Cryogenic Performance of the Spoke Prototype Cryomodule for ESS. FREIA Report 2019/05, Uppsala University, 2019.
- [53] H. Li et al. RF Performance of the Spoke Prototype Cryomodule for ESS. FREIA Report 2019/08, Uppsala University, 2019.
- [54] S. Verdu-Andres et al. Design and vertical tests of double-quarter wave cavity prototypes for the high-luminosity LHC crab cavity system. *Phys. Rev. Accel. Beams*, 21:082002, 2018.
- [55] A. Miyazaki et al. First cold test of a crab cavity at the GERSEMI cryostat for the HL-LHC project. arXiv:2011.05210 [physics.acc-ph], 2020.
- [56] A. Ballarino. Development of superconducting links for the large hadron collider machine. *Superconductor Science and Technology*, 27(4):044024, 2014.
- [57] D.I. Meyer and R. Flasck. A new configuration for a dipole magnet for use in high energy physics applications. *Nucl. Instr. and Meth.*, 80:339, 1970.
- [58] G. Kirby et al. Hi-Lumi LHC Twin Aperture Orbit Correctors 0.5 m Magnet Assembly and Cold Test. *IEEE Trans. Appl. Supercond.*, 28(3):4002205, 2018.
- [59] M. Jacewicz et al. Spectrometers for RF breakdown studies for CLIC. *Nucl. Instr. and Meth.*, A828:63, 2016.
- [60] M. Jacewicz et al. Temperature-Dependent Field Emission and Breakdown Measurements Using a Pulsed High-Voltage Cryosystem. *Phys.Rev.Applied*, 14:061002, 2020.
- [61] A. Mak, P. Salén, and V. Goryashko. Compact undulator line for a high-brilliance soft-x-ray free-electron laser at MAX IV. *Journal of Synchrotron Radiation*, 26(3):891–898, April 2019.
- [62] F. Curbis et al. Status of the soft x-ray laser (sxl) project at max iv laboratory. In *Proc. of the 39th Free Electron Laser Conference FEL15* [72], page 749.
- [63] G. D’Auria et al. Status of the CompactLight Design Study. In *Proc. of the 39th Free Electron Laser Conference FEL15* [72], page 738.
- [64] R. Tong, S. Book, L.H. Duc, and D. Dancila. A Planar Single-ended Kilowatt-level VHF Class E Power Amplifier. In *2019 14th European Microwave Integrated Circuits Conference (EuMIC)*, page 338. IEEE, 2019.
- [65] R. Tong, O. Bengtsson, A. Bäcklund, and D. Dancila. Compact and Highly Efficient Kilowatt Lumped Push-Pull Power Amplifier for Cyclotron in Radioisotopes Production. *IEEE Trans. Microw. Theory Tech.*, 69 (1):723, 2021.
- [66] I. Aziz et al. Effects of proton irradiation on 60 GHz CMOS transceiver chip for multi-Gbps communication in high-energy physics experiments. *J. Eng.*, 8:5391, 2019.
- [67] I. Aziz et al. 60 GHz Compact broadband antenna arrays with wide-angle beam steering. *J. Eng.*, 8:5407, 2019.
- [68] E. Wildner et al. The Opportunity Offered by the ESSnuSB Project to Exploit the Larger Leptonic CP Violation Signal at the Second Oscillation Maximum and the Requirements of This Project on the ESS Accelerator Complex. *Advances in High Energy Physics*, 2016:16, 2016.

- [69] Accelerator Research and Innovation for European Science and Society (ARIES). Project web page <http://cern.ch/aries>.
- [70] IPAC 2014. *International Particle Accelerator Conference*, June 2014, Dresden, Germany.
- [71] IPAC 2017. *International Particle Accelerator Conference*, May 2017, Copenhagen, Denmark.
- [72] FEL 2019. *International Free Electron Laser Conference*, August 2019, Hamburg, Germany.